Adv Comput Math (2018) 44:1475–1518
https://doi.org/10.1007/s10444-018-9594-8

Large deformation shape uncertainty quantification in acoustic scattering

R. Hiptmair[1] · L. Scarabosio[2] · C. Schillings[3] · Ch. Schwab[1]

Received: 2 February 2017 / Accepted: 16 February 2018
Published online: 16 March 2018

Abstract We address shape uncertainty quantification for the two-dimensional Helmholtz transmission problem, where the shape of the scatterer is the only source of uncertainty. In the framework of the so-called deterministic approach, we provide a high-dimensional parametrization for the interface. Each domain configuration is mapped to a nominal configuration, obtaining a problem on a fixed domain with stochastic coefficients. To compute surrogate models and statistics of quantities of interest, we apply an adaptive, anisotropic Smolyak algorithm, which allows to attain high convergence rates that are independent of the number of dimensions activated in the parameter space. We also develop a regularity theory with respect to the spatial variable, with norm bounds that are independent of the parametric dimension. The techniques and theory presented in this paper can be easily generalized to any elliptic problem on a stochastic domain.

Communicated by: Ivan Graham

✉ L. Scarabosio
scarabos@ma.tum.de

R. Hiptmair
hiptmair@sam.math.ethz.ch

C. Schillings
c.schillings@uni-mannheim.de

Ch. Schwab
schwab@sam.math.ethz.ch

[1] Seminar for Applied Mathematics, D-MATH, ETH Zurich, Zurich, Switzerland

[3] Department of Mathematics, Chair of Numerical Mathematics, Technical University of Munich, Munich, Germany

[3] Institut für Mathematik, Fakultät für Wirtschaftsinformatik & Wirtschaftsmathematik, Universität Mannheim, Mannheim, Germany

Keywords Uncertainty quantification · Random interface · Stochastic parametrization · High-dimensional approximation · Helmholtz equation · Dimension-adaptive Smolyak quadrature

Mathematics Subject Classification (2010) 35R60 · 60H35 · 65N75 · 65N12

1 Introduction

In nano-optics applications, imperfections in the manufacturing process may lead to a considerable uncertainty in the shape of nano-devices. The aim of the present work is to quantify how such shape variations affect the optical response of a nano-sized scatterer to some electromagnetic excitation. Our focus is on the estimation of surrogate models (interpolation) and statistics (quadrature) of quantities of interest (Q.o.I.s).

Since the shape fluctuations cannot be considered to be small compared to the scatterer size, a perturbative approach [17, 27, 29] is not suitable for our framework. On the other hand, the slow convergence rate of Monte Carlo sampling renders it computationally inefficient for such kind of applications, since each sample would require the numerical solution of a full electromagnetic field problem. The multilevel version of the Monte Carlo algorithm (MLMC) would still require a massive computational effort in order to reach a certain accuracy. Furthermore, Monte Carlo methods, while being very simple as quadrature rules, are not well suited for interpolation.

Instead, in the present work we model the uncertain shape through a *high-dimensional parametrization approach*, and then apply an algorithm for interpolation and quadrature that, exploting some regularity properties of the Q.o.I., allows to achieve convergence rates which are much higher than the ones attainable with Monte Carlo algorithms and do not suffer from the so-called 'curse of dimensionality'.

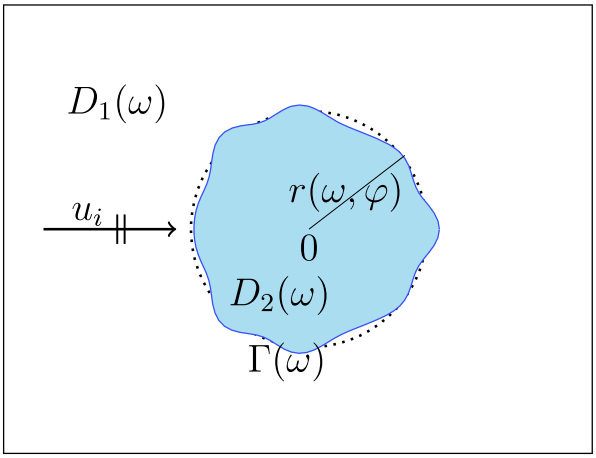

Fig. 1 Particle in free space

We illustrate the method on a two-dimensional *Helmholtz transmission problem* with an incoming plane wave, where the material parameters are assumed to be known exactly; the shape of the scatterer is thus the only source of uncertainty. We focus on the case of a particle in free space, whose geometry is depicted in Fig. 1.

1.1 Model problem

Let $(\Omega, \mathcal{A}, \mathbb{P})$ be a probability space, with $\mathcal{A}$ a σ-algebra on the set Ω and $\mathbb{P}$ a probability measure on $(\Omega, \mathcal{A})$. For every $\omega \in \Omega$, we formally define $\Gamma(\omega)$ to be the boundary of the scatterer, $D_1(\omega)$ the exterior unbounded domain, and $D_2(\omega)$ the domain occupied by the scatterer. We assume that $D_1(\omega) \cup \Gamma(\omega) \cup D_2(\omega) = \mathbb{R}^2$ for every $\omega \in \Omega$.

The transmission problem for the Helmholtz equation can be written as

$$\begin{cases} -\nabla \cdot (\alpha(\Gamma(\omega), \boldsymbol{x})\nabla u) - \kappa^2(\Gamma(\omega), \boldsymbol{x})u = 0 \quad \text{in } \mathbb{R}^2, & \text{(1.1a)} \\ [\![u]\!]_{\Gamma(\omega)} = 0, \quad [\![\alpha(\Gamma(\omega), \boldsymbol{x})\nabla u \cdot \boldsymbol{n}]\!]_{\Gamma(\omega)} = 0, & \text{(1.1b)} \\ \lim\limits_{|\boldsymbol{x}|\to\infty} \sqrt{|\boldsymbol{x}|}\left(\dfrac{\partial}{\partial\,|\boldsymbol{x}|} - i\kappa_1\right)(u(\omega) - u_i)(\boldsymbol{x}) = 0, & \text{(1.1c)} \\ \text{for every } \omega \in \Omega, \end{cases}$$

with uniformly positive, real-valued, piecewise-constant coefficients in each subdomain:

$$\alpha(\Gamma(\omega), \boldsymbol{x}) = \begin{cases} 1 & \text{if } \boldsymbol{x} \in D_1(\omega), \\ \alpha_2 & \text{if } \boldsymbol{x} \in D_2(\omega), \end{cases} \qquad \kappa^2(\Gamma(\omega), \boldsymbol{x}) = \begin{cases} \kappa_1^2 & \text{if } \boldsymbol{x} \in D_1(\omega), \\ \alpha_2\,\kappa_2^2 & \text{if } \boldsymbol{x} \in D_2(\omega). \end{cases} \tag{1.2}$$

The unknown $u = u(\omega, \boldsymbol{x})$ represents the total field, whereas κ_1 and κ_2 denote the wavenumbers in free space and in the scatterer, respectively; α_2 is a positive real coefficient. In equation (1.1b), the symbol $[\![\cdot]\!]_{\Gamma(\omega)}$ denotes the jump across the random interface $\Gamma(\omega)$. Equation (1.1c) is the so-called Sommerfeld radiation condition, where $u_i(\boldsymbol{x}) = e^{i\kappa_1 \boldsymbol{d}\cdot\boldsymbol{x}}$ is the incoming plane wave, with $\boldsymbol{d}$ a unit vector indicating the direction of propagation. The Sommerfeld radiation condition corresponds to the radiation condition in free space.

We work in the *large wavelength regime*, which excludes the presence of resonant geometric structures. Thus, the results of this paper are not restricted to the Helmholtz equation, but hold for any elliptic equation.

The two-dimensional Helmholtz equation describes the scattering of an electromagnetic wave from a cylinder of infinite length, and the unknown u corresponds to the out-of-plane component of the electric field (TE mode) or of the magnetic field (TM mode), depending on the meaning conferred to the coefficients in the equation (see e.g. [41]). The same results and methodology presented in this paper, however, still hold for the three-dimensional Helmholtz equation, when the Fourier harmonics used to model the shape variations (see Section 2) are replaced by spherical harmonics.

1.2 Outline and related work

The parametric approach to represent the uncertainty was developed by Ghanem and Spanos (e.g. [24]) from the pioneering ideas of Wiener [47]. In this framework, in Section 2 we give a probabilistic description of the interface $\Gamma = \Gamma(\omega)$, so that it will then depend on $\omega \in \Omega$ indirectly through a deterministic, high-dimensional parameter representing the stochasticity. In particular, we express the variations of the scatterer boundary through an affine combination of a finite number of independent, uniformly distributed random variables, as it is commonly done to model the stochastic diffusion coefficient in the scalar diffusion model (see [12, 13, 45], just to mention some). Such an expansion can be regarded as an approximation to the exact probability distribution of the interface [49].

In Section 3, we use the domain mapping approach introduced by Xiu and Tartakovsky in [46, 49] to map each domain realization to a nominal configuration, fixed for all realizations, using a parameter-dependent map. A similar technique has been adopted in [8] and [28] too. In the latter articles, the authors model the shape uncertainty through a Karhunen-Loève expansion of the map from a reference configuration to the physical, in contrast to our work which separates the stochastic description of the interface, provided in Section 2, from the mapping itself. We let randomness enter through the interface model and then it propagates to the map. Alternative methods to the domain mapping are the fictitious domain approach introduced by Canuto and Kozubek in [7] and the level set methods developed by Nouy et al. in [39]. For two reasons we prefer the mapping approach. First, this approach facilitates the theoretical analysis of the regularity of the solution (with respect to both the high-dimensional parameter and the spatial coordinate). Second, when using the fictitious domain approach or the level set method, the solution is not smooth with respect of the high-dimensional parameter at the domain boundary. Conversely, the domain mapping allows us, in Section 4, to write a variational formulation for (1.1) on the *nominal* configuration with parameter-dependent coefficients, bringing the problem to a framework for which theory and discretization algorithms are well established and can be applied without modifications.

In Section 5, we address the discretization of the latter variational formulation with respect to the parameter representing the stochasticity. Two main methods can be used: the stochastic Galerkin and the stochastic collocation methods.

The stochastic Galerkin approach (see [45] for a comprehensive review), due to its intrusive nature (at least in its original version), is not well suited for our application, where the coefficients of the PDE (partial differential equation) depend nonlinearly on the high-dimensional parameter. We use instead sparse collocation, introduced independently by Babuška, Nobile and Tempone in [2] and by Xiu and Hesthaven in [48]. To overcome the so-called *curse of dimensionality* due to the high dimension of the parameter space, we use the sparse adaptive Smolyak algorithm for stochastic quadrature and interpolation described in [43], and pioneered in the earlier work [23] of Gerstner and Griebel. This is shown to achieve convergence rates independent of the number of dimensions considered.

In the same section we also discuss the fulfillment, in our framework, of the key assumption of all convergence theorems, that is the holomorphy of the Q.o.I.

(e.g. the solution to (1.1) or linear functionals of it) with respect to an extension of the high-dimensional parameter to the complex plane. Due to the domain transformation introduced in Section 4, we need a stronger regularity constraint for the scatterer boundary than the one that is usually needed for the diffusion coefficient in elliptic problems on deterministic domains. Similar regularity results are shown in [28] and [8]. However, [28] addresses the smoothness of the Q.o.I. with respect to the real-valued parameter, whose analysis is different than when the parameter is complex-valued. In [8], the smoothness results refer to the holomorphic extension of the Q.o.I. to complex polyellipses, in view of the application of an isotropic sparse grid algorithm. Nevertheless, we believe that our regularity analysis is still of interest for two reasons. First, differently from [8] and [28], we emphasize the anisotropy of the region of holomorphy with respect to the dimension, because this is the key property that determines the convergence rate of our anisotropic, dimension-robust sparse grid algorithm. Second, in our case the regularity of the solution is obtained not from specific direct calculations depending on the variational formulation, as it is the case in [8] and [28], but from a more general result from [10] based on implicit differentiation, so that our approach is more easily generalizable to a wide class of PDEs. Our results on the holomorphy of the solution rely on a specific parametrization of the scatterer boundary, but it has been recently shown in [14], in the framework of stationary Navier-Stokes equations and in [32] for Maxwell's equations, that this is a particular case of *shape holomorphy*, which holds for a wider class of domain transformations.

Section 6 is, in our opinion, one of the major contributions of this paper. There, we address the space discretization on the nominal configuration and couple it to the results of the previous section. For the spatial problem, we use a finite element discretization. We point out that a boundary element formulation (as used, for example, in [29]) is not applicable in the context of the mapping approach, due to variable coefficients in the resulting variational formulation. Of course, the boundary element method can be used on the mapped domain, but a straightforward implementation would require reassembly of the system matrix for every realization, leading to high computational costs. Thus, in Section 6, after discussing space regularity results for the solution at each collocation point, we couple finite element convergence estimates to convergence estimates for sparse interpolation and quadrature, obtaining convergence results for the solution to the fully discretized problem and linear output functionals. We first consider the simpler case of uniform finite element discretization for all the parameter realizations, and then the case when different space discretizations are used for different collocation points. For the former approach, the procedure that we present is quite similar to the one presented in [8]. There, however, the convergence rates presented for the sparse grid error are not independent of the number of dimensions involved, and the effect of the amplitude of the stochastic perturbations on the smoothness of the solution and thus on the convergence rate of the finite element discretization is not taken into account. The results that we obtain for the case that the space discretization is different for each collocation point can be thought as a starting point for a parameter-adaptive space discretization to reduce the global computational effort [4, 19].

In Section 7, we show that in numerical experiments we achieve, and even surpass, the predicted theoretical convergence rates for both sparse interpolation and sparse quadrature on the nominal configuration.

2 Parametrization of the interface

In the first subsection, we give a probabilistic model for the interface Γ. Using such probabilistic characterization, in the second subsection we convert the stochastic problem to a deterministic problem on a high-dimensional parameter domain. This approach is particularly relevant in the perspective of a discretization, since we will see that, differently from the probability space Ω, the space where the deterministic parameter lives is suitable for discretization.

2.1 Probabilistic modeling of the interface

In order to have a simple representation of the interface, we require:

Assumption 2.1 *For every $\omega \in \Omega$, the domain $D_2(\omega)$ is star-shaped with respect to the origin and the interface $\Gamma(\omega)$ is of class C^1.*

In this way, $D_2(\omega)$ can be fully described by a stochastic, angle-dependent radius $r = r(\omega, \varphi) \in C^k_{\text{per}}([0, 2\pi))$ for every $\omega \in \Omega$ and some $k \geq 1$, representing the interface $\Gamma = \Gamma(\omega)$. The techniques we are going to present can be extended to the case of an interface that is only piecewise of class C^k ($k \geq 1$), but for ease of treatment we do not consider this case.

As it is commonly done in the framework of partial differential equations with stochastic diffusion coefficient (see e.g. [12, 13, 45]), we expand the uncertain radius as:

$$r(\omega, \varphi) = r_0(\varphi) + \sum_{j=1}^{J} c_j Y_{2j-1}(\omega) \cos(j\varphi) + s_j Y_{2j}(\omega) \sin(j\varphi), \quad \varphi \in [0, 2\pi), \ J \in \mathbb{N}, \omega \in \Omega. \tag{2.1}$$

In this formal expression, $r_0 = r_0(\varphi) \in C^k_{\text{per}}([0, 2\pi))$, $k \geq 1$, is referred to as the nominal shape, and it can be considered as an approximate parametrization of the mean shape. The truncation of the expansion in (2.1), commonly referred to in the literature [2] as *finite noise assumption*, reflects the fact that, when reconstructing the expansion (2.1) from measurements, only a finite number of Fourier coefficients can be estimated. In the following, in particular in Section 6, we will ensure that all the estimates we will obtain hold *uniformly* in the truncation parameter $J \in \mathbb{N}$.

The random variables $\{Y_j\}_{j\geq 1}^{2J}$ are assumed to satisfy:

Assumption 2.2 $\{Y_j\}_{j\geq 1}^{2J}$ *are i.i.d. with $Y_j \sim \mathcal{U}([-1, 1])$ for every $1 \leq j \leq 2J$ and every $J \in \mathbb{N}$.*

In particular $\{Y_j\}_{j\geq 1}^{2J}$ have compact image, namely $|Y_j| \leq 1$ for every j. Thus, the only way to have a J-independent bound on the radius expansion (2.1) and a decay of its Fourier coefficients is to impose some constraints on the real coefficient sequences.

To ensure boundedness and positivity of the stochastic radius r at each angle φ and for every $\omega \in \Omega$, we require that $r = r(\omega, \varphi)$ varies inside the range $[\frac{r_0(\varphi)}{2}, \frac{3r_0(\varphi)}{2}]$:

Assumption 2.3 *The coefficient sequences $\mathcal{C} := (c_j)_{j\geq 1}$ and $\mathcal{S} := (s_j)_{j\geq 1}$ satisfy*

$$\sum_{j\geq 1}(|c_j| + |s_j|) \leq \frac{r_0^-}{2},$$

with $r_0^- = inf_{\varphi\in[0,2\pi)} r_0(\varphi) > 0$.

For the Fourier coefficients, we require them to have a 'sufficiently fast' polynomial decay:

Assumption 2.4 *The sequences $\mathcal{C}$ and $\mathcal{S}$ have a monotonically decreasing majorant which belongs to $\ell^p(\mathbb{N})$ with $0 < p < \frac{1}{2}$, and the sequences $(j|c_j|^p)_{j\geq 1}$ and $(j|s_j|^p)_{j\geq 1}$ have a monotonically decreasing majorant.*

As it may be expected from harmonic analysis results, the decay of the coefficient sequences determines the regularity of the radius:

Lemma 2.5 *If the coefficient sequences $\mathcal{C}$, $\mathcal{S}$ satisfy* Assumption 2.4*, then the radius $r = r(\omega, \varphi)$ given by* (2.1) *satisfies*

$$\|r(\omega)\|_{C^k_{per}([0,2\pi))} \leq C(\mathcal{C}, \mathcal{S}), \quad \text{for every } \omega \in \Omega, \tag{2.2}$$

under the assumption that also the nominal radius r_0 belongs to $C^k_{per}([0, 2\pi))$. The constant C depends on the regularity parameter k and on the sequences $\mathcal{C} = (c_j)_{j\geq 1}$ and $\mathcal{S} = (s_j)_{j\geq 1}$, but not on the truncation dimension $J \in \mathbb{N}$ and on $\omega \in \Omega$. The regularity parameter k is given by:

$$k = \begin{cases} \left\lfloor \frac{1}{p} - 1 \right\rfloor & \text{if } \frac{1}{p} - 1 \text{ is not an integer,} \\ \frac{1}{p} - 2 & \text{otherwise.} \end{cases} \tag{2.3}$$

Proof The proof consists of elementary computations and we refer to [42, Lemma C.0.5] for it. □

Remark 2.6 Equation (2.1) can be rewritten as

$$r(\omega, \varphi) = r_0(\varphi) + \sum_{l=1}^{L} \beta_l Y_l(\omega)\psi_l(\varphi), \quad \varphi \in [0, 2\pi), \quad L \in \mathbb{N}, \tag{2.4}$$

with $\psi_l = \cos(\frac{l+1}{2}\varphi)$ and $\beta_l = c_{\frac{l+1}{2}}$ if l is odd, $\psi_l = \sin(\frac{l}{2}\varphi)$ and $\beta_l = s_{\frac{l}{2}}$ if l is even. The truncation L is given by $L = 2J$, with J as in (2.1).

In general, any basis $(\psi_l)_{l\geq 1}$ of $L^2_{\mathrm{per}}([0,2\pi))$ could be considered, provided that $\psi_l \in C^1_{\mathrm{per}}([0,2\pi))$ for each $l \geq 1$. Nevertheless, the choice of the Fourier basis is particularly relevant in view of possible applications, when, for instance, r_0 is a circle and (2.4) is obtained from the Karhunen-Loève expansion of a rotationally invariant covariance kernel.

2.2 Parametric formulation

In this subsection we recall via application to our case the standard parametrization procedure followed in stochastic Galerkin and stochastic collocation frameworks; we refer to [45] for an exhaustive survey of the topic.

From Assumption 2.2, we know that for each random variable $Y_j : \Omega \to \mathcal{P}_j$, $1 \leq j \leq 2J$, with $\mathcal{P}_j = [-1,1]$ endowed with the Borel σ-algebra Σ_j, the distribution μ_j of Y_j is the uniform distribution. Then the sequence $\left(Y_j\right)_{j\geq 1}^{2J}$ defines a map

$$\boldsymbol{Y} : \Omega \to \mathcal{P}_J := \bigotimes_{j=1}^{2J} \mathcal{P}_j = [-1,1]^{2J}, \quad \omega \mapsto \left(Y_j(\omega)\right)_{j=1}^{2J}, \tag{2.5}$$

measurable with respect to the product σ-algebra $\Sigma := \bigotimes_{j=1}^{2J} \Sigma_j$ on $\mathcal{P}_J$. $\mathcal{P}_J$ is commonly referred to as the *parameter space*.

The random variables Y_j being independent, the distribution of $\boldsymbol{Y}$ is the product probability measure $\mu := \bigotimes_{j=1}^{2J} \mu_j$. In particular, under Assumption 2.2, $\mu = \left(\frac{1}{2}\right)^{2J}$.

Now, we denote by $\boldsymbol{y} = \left(y_j\right)_{j=1}^{2J} \in \mathcal{P}_J$ one realization of the random variable $\boldsymbol{Y}$, so that we can rewrite (2.1) as

$$\begin{aligned} r(\boldsymbol{y},\varphi) &= r_0(\varphi) + \sum_{j=1}^{J} c_j y_{2j-1} \cos(j\varphi) + s_j y_{2j} \sin(j\varphi), \\ \boldsymbol{y} &= \left(y_j\right)_{j=1}^{2J} \in \mathcal{P}_J,\ \varphi \in [0,2\pi). \end{aligned} \tag{2.6}$$

Remark 2.7 In Assumption 2.2, the uniform distribution hypothesis for the random variables serves as a model and can be easily relaxed (see Section 9.1 in [42]). The requirement that the random variables are mutually independent is instead harder to drop. This is due to the fact that, if such condition is not fulfilled, then the joint probability distribution μ cannot be expressed as product of the univariate distributions anymore and, as mentioned in [42, Sect. 9.1], one would need to adapt the theoretical convergence analysis under some assumptions on μ.

3 Mapping to nominal geometry

In the first subsection we give a general description of the approach, while in the second subsection we apply it to our specific case of a particle in free space.

3.1 General description

To overcome the unboundedness of the domain, consider, in the domain with interface $\Gamma(\boldsymbol{y})$, a circle ∂K_R of arbitrary radius R containing the scatterer $D_2(\boldsymbol{y})$ in its interior. We choose ∂K_R to be *fixed for all realizations* $\boldsymbol{y} \in \mathcal{P}_J$, $J \in \mathbb{N}$, and we denote by K_R the region enclosed inside ∂K_R, no matter which realization $\Gamma(\boldsymbol{y})$ of the interface is considered.

Following the approach introduced, for instance, in [10, 28] and [49], we consider a *nominal configuration* of the domain K_R, where the interface $\hat{\Gamma}$ is *fixed*, i.e. independent of the realization $\boldsymbol{y}$, and a bijective parameter-dependent mapping

$$\begin{aligned} \Phi(\boldsymbol{y}): \quad K_R &\longrightarrow K_R \\ (\hat{x}_1, \hat{x}_2) &\mapsto (x_1, x_2) \end{aligned} \tag{3.1}$$

from the nominal configuration to the domain K_R with interface $\Gamma(\boldsymbol{y})$.

A possible choice for $\hat{\Gamma}$ is the interface associated with the nominal radius r_0, or, in other words, to the case when $\boldsymbol{y} = \mathbf{0}$. We denote by $\hat{D}_2$ the scatterer region when the interface is $\hat{\Gamma}$, and $\hat{D}_1 := \mathbb{R}^2 \setminus \hat{D}_2$. In order to preserve the well-posedness of the problem as it will be discussed in Section 4, we formulate the following assumptions on Φ:

Assumption 3.1 *For every $J \in \mathbb{N}$, every $\boldsymbol{y} \in \mathcal{P}_J$ and an integer $k \geq 1$, the mapping $\Phi(\boldsymbol{y}) : K_R \to K_R$ fulfills the following properties:*

(i) *$\Phi(\boldsymbol{y})$ is a C^k-orientation preserving diffeomorphism in each of the two subdomains $\hat{D}_1 \cap K_R$ and $\hat{D}_2$, with uniformly bounded norms, i.e.:*
$\|\Phi(\boldsymbol{y})\|_{C^k_{\hat{pw}}(\overline{K_R})} \leq C_1, \quad \|\Phi^{-1}(\boldsymbol{y})\|_{C^k_{pw_{\boldsymbol{y}}}(\overline{K_R})} \leq C_2, \quad$ *for all $J \in \mathbb{N}$ and all $\boldsymbol{y} \in \mathcal{P}_J$,*

where C_1 and C_2 are independent of the truncation dimension $J \in \mathbb{N}$ and of $\boldsymbol{y} \in \mathcal{P}_J$, and $\|\cdot\|_{C^k_{\hat{pw}}(\overline{K_R})} := \|\cdot\|_{C^k(\overline{\hat{D}_1 \cap K_R}) \cup C^k(\overline{\hat{D}_2})} = \|\cdot\|_{C^k(\overline{\hat{D}_1 \cap K_R})} + \|\cdot\|_{C^k(\overline{\hat{D}_2})}$ (similarly in $\|\cdot\|_{C^k_{pw_{\boldsymbol{y}}}(\overline{K_R})}$ the discontinuities are allowed across $\Gamma(\boldsymbol{y})$).

(ii) *$\Phi(\boldsymbol{y})$ is the identity on ∂K_R:*

$$\Phi(\boldsymbol{y}, \hat{\boldsymbol{x}}) = \hat{\boldsymbol{x}} \text{ for all } \hat{\boldsymbol{x}} \in \partial K_R \text{ and all } J \in \mathbb{N},\ \boldsymbol{y} \in \mathcal{P}_J.$$

From Assumption 3.1 (i), using the Courant-Fischer theorem for singular values [31, Thm. 3.1.2] we deduce immediately the following lemma.

Lemma 3.2 *Let $\sigma_1 = \sigma_1(\boldsymbol{y}, \boldsymbol{x})$, $\sigma_2 = \sigma_2(\boldsymbol{y}, \boldsymbol{x})$ be the singular values of $D\Phi^{-1}(\boldsymbol{y})$ (the Jacobian matrix of Φ^{-1}). Under* Assumption 3.1 (i)*, there exist constants σ_{min}, $\sigma_{max} > 0$, independent of the truncation dimension $J \in \mathbb{N}$ and of $\boldsymbol{y} \in \mathcal{P}_J$, such that*

$$\sigma_{min} \leq \|\sigma_1(\boldsymbol{y}, \cdot)\|_{C^0_{pw_{\boldsymbol{y}}}(\overline{K_R})}, \|\sigma_2(\boldsymbol{y}, \cdot)\|_{C^0_{pw_{\boldsymbol{y}}}(\overline{K_R})} \leq \sigma_{max} \quad \text{for all } J \in \mathbb{N},\ \boldsymbol{y} \in \mathcal{P}_J$$

(or, equivalently, analogous bounds hold for the singular values of $D\Phi(\boldsymbol{y})$, the Jacobian matrix of Φ).

3.2 The domain mapping for a particle in free space

In this case, we choose $r_0(\varphi)$ as the boundary of the scatterer in the nominal configuration, and map it to the boundary of the actual scatterer. The movement of the interface is propagated in the regions inside and outside the scatterer using a mollifier. In formulae, we have:

$$\boldsymbol{x}(\boldsymbol{y}) = \Phi(\boldsymbol{y}, \hat{\boldsymbol{x}}) = \hat{\boldsymbol{x}} + \chi\left(\hat{\boldsymbol{x}}\right)\left(r(\boldsymbol{y}, \hat{\varphi}_{\hat{\boldsymbol{x}}}) - r_0(\hat{\varphi}_{\hat{\boldsymbol{x}}})\right)\frac{\hat{\boldsymbol{x}}}{\|\hat{\boldsymbol{x}}\|}, \tag{3.2}$$

with $\hat{\varphi}_{\hat{\boldsymbol{x}}} := \arg(\hat{\boldsymbol{x}}) = \arg(\boldsymbol{x}) = \varphi$. The mollifier $\chi : K_R \to \mathbb{R}_{0,+} := \mathbb{R}_+ \cup \{0\}$ satisfies the following conditions:

- $\chi(\hat{\boldsymbol{x}}) = \chi(\|\hat{\boldsymbol{x}}\|, r_0)$, that is, χ acts on the radial component of $\hat{\boldsymbol{x}} \in K_R$, and its dependence on the angle $\hat{\varphi}$ is only due to the fact that it depends on $r_0 = r_0(\varphi)$, $\varphi \in [0, 2\pi)$;
- $0 \le \chi(\hat{\boldsymbol{x}}) \le 1$, $\hat{\boldsymbol{x}} \in K_R$, with $\chi(\hat{\boldsymbol{x}}) = 0$ for $\|\hat{\boldsymbol{x}}\| \le \frac{r_0^-}{4}$ (r_0^- being the quantity defined in Assumption 2.3) and for $\|\hat{\boldsymbol{x}}\| \ge \tilde{R}$ ($\tilde{R} \in \mathbb{R}$, $\sup_{[0,2\pi)} r_0(\varphi) + \frac{r_0^-}{2} < \tilde{R} \le R$), and with $\chi(\hat{\boldsymbol{x}}) = 1$ for $\|\hat{\boldsymbol{x}}\| = r_0$;
- χ is globally continuous and is monotonically increasing for $\frac{r_0^-}{4} \le \|\hat{\boldsymbol{x}}\| \le r_0(\varphi)$ and monotonically decreasing for $r_0(\varphi) \le \|\hat{\boldsymbol{x}}\| \le \tilde{R}$.

The map is illustrated in Fig. 2. We also require:

Assumption 3.3 *The mollifier χ in (3.2) has in $\hat{D}_2$ and in $\hat{D}_1 \cap K_R$ at least the same smoothness as the nominal radius r_0 has in $[0, 2\pi)$. Furthermore,* $\max\left\{\|\chi\|_{C^1(\hat{D}_2)}, \|\chi\|_{C^1(\hat{D}_1 \cap K_R)}\right\} \le C_\chi$, *where $C_\chi \in \mathbb{R}$ is such that $0 < C_\chi < \frac{1}{\sqrt{2}\left(\frac{r_0^-}{2} + c_\chi\right)}$ for some $c_\chi > 0$.*

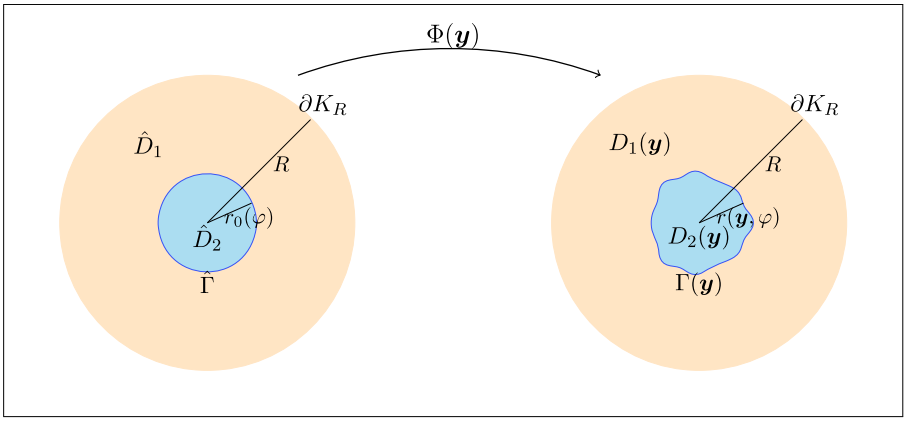

Fig. 2 Mapping for the case of particle in free space

Lemma 3.4 *Let Assumptions 2.3 and 2.4 be satisfied, and let the nominal radius* r_0 *belong to* $C^k_{per}([0, 2\pi))$*, with* k *as in* (2.3)*. If we choose* χ *according to Assumption 3.3, then the mapping* Φ *given by* (3.2) *satisfies Assumption 3.1, with* k *the smoothness parameter of the radius* r*.*

Proof The statement is quite clear from (3.2), once one observes that $\Phi(\boldsymbol{y})$ consists just of scalings by $r(\boldsymbol{y})$ and r_0 smoothed by a function χ with the same smoothness as the nominal radius. The technical proof can be found in [42], Appendix E. □

For the implementation, it is not easy to find a mollifier for the mapping (3.2) that fulfills Assumption 3.3 and such that Φ and its inverse have a closed form. What one can do instead is to relax Assumption 3.3. Namely, in (3.2) we use:

$$\chi(\hat{\boldsymbol{x}}) = \begin{cases} 0 & \text{if } \|\hat{\boldsymbol{x}}\| \leq \frac{r_0^-}{4}, \\ \frac{\|\hat{\boldsymbol{x}}\| - \frac{r_0^-}{4}}{r_0(\hat{\varphi}_{\hat{\boldsymbol{x}}}) - \frac{r_0^-}{4}} & \text{if } \frac{r_0^-}{4} < \|\hat{\boldsymbol{x}}\| \leq r_0(\hat{\varphi}_{\hat{\boldsymbol{x}}}), \\ \frac{R - \|\hat{\boldsymbol{x}}\|}{R - r_0(\hat{\varphi}_{\hat{\boldsymbol{x}}})} & \text{if } r_0(\hat{\varphi}_{\hat{\boldsymbol{x}}}) \leq \|\hat{\boldsymbol{x}}\| \leq R. \end{cases} \tag{3.3}$$

It is clear that the mollifier above does not fulfill Assumption 3.3, because the mapping Φ is not a C^k-diffeomorphism in $\hat{D}_2$. However, denoting $\hat{D}_2^{in} := \left\{\hat{\boldsymbol{x}} \in \hat{D}_2 : \|\hat{\boldsymbol{x}}\| < \frac{r_0^-}{4}\right\}$, we have that Φ is a C^k-diffeomorphism piecewise, in $\hat{D}_2^{in}$ and $\hat{D}_2 \setminus \hat{D}_2^{in}$. With such a property, we will see in the following sections that, using some caution, the theory would still work (see Remark 6.8).

The multiplication by a mollifier is not the only way of propagating the movement of the interface. Among the valid alternatives we mention the use of a harmonic extension [35, 49] or of level set methods [1, 40].

4 Variational formulation and well-posedness of the model problem

In the first part of this section we derive the variational formulation for the model problem (1.1), while in the second part we address its well-posedness (in Hadamard's sense).

4.1 Variational formulation

As in the previous section, we consider the space K_R enclosed inside a circle of radius $R > 0$, the latter *fixed for all realizations* $\boldsymbol{y} \in \mathcal{P}_J$, and containing the scatterer in its interior (see Fig. 3). Then, using the Dirichlet-to-Neumann map (DtN, see [38, Sect. 2.6.3]), we can state the variational formulation for (1.1) on the *bounded* domain K_R. Applying the parametric description of the uncertain interface developed in Section 2, we obtain:

$$
\begin{aligned}
&\text{Find } u(\boldsymbol{y}) \in V :\\
&a_y(u(\boldsymbol{y}), v) := \int_{K_R} \alpha(\boldsymbol{y}, \boldsymbol{x})\, \nabla u(\boldsymbol{y}) \cdot \nabla v - \kappa^2(\boldsymbol{y}, \boldsymbol{x})\, u(\boldsymbol{y}) \cdot v \, d\boldsymbol{x}\\
&\qquad\qquad - \int_{\partial K_R} DtN(u(\boldsymbol{y}))v \, dS\\
&\qquad\qquad = \int_{\partial K_R} \left(-DtN(u_i) + \frac{\partial u_i}{\partial \boldsymbol{n}_R} \right) v \, dS \quad \text{for all } v \in V \text{ and all } \boldsymbol{y} \in \mathcal{P}_J,
\end{aligned}
\tag{4.1}
$$

where $V := H^1(K_R)$ and $\boldsymbol{n}_R$ is the outer normal to K_R.

Now, we use the inverse of the map $\Phi(\boldsymbol{y})$, $\boldsymbol{y} \in \mathcal{P}_J$, introduced in Section 3, to map the physical configuration, with interface $\Gamma(\boldsymbol{y})$, to the nominal configuration, with interface $\hat{\Gamma}$. Reordering the terms, we obtain the following parametric, variational formulation on the *fixed*, deterministic configuration with interface $\hat{\Gamma}$:

$$
\begin{aligned}
&\text{Find } \hat{u}(\boldsymbol{y}) \in \hat{V} :\\
&\hat{a}_y(\hat{u}(\boldsymbol{y}), \hat{v}) = \int_{K_R} \hat{\alpha}(\boldsymbol{y}, \hat{\boldsymbol{x}})\, \hat{\nabla} \hat{u}(\boldsymbol{y}) \cdot \hat{\nabla} \hat{v} \, d\hat{\boldsymbol{x}} - \hat{\kappa}^2(\boldsymbol{y}, \hat{\boldsymbol{x}})\, \hat{u}(\boldsymbol{y}) \cdot \hat{v} \, d\hat{\boldsymbol{x}}\\
&\qquad\qquad - \int_{\partial K_R} DtN(\hat{u}(\boldsymbol{y}))\hat{v} \, dS\\
&\qquad\qquad = \int_{\partial K_R} \left(-DtN(u_i) + \frac{\partial u_i}{\partial \boldsymbol{n}_R} \right) \hat{v} \, dS \quad \text{for all } \hat{v} \in \hat{V} \text{ and all } \boldsymbol{y} \in \mathcal{P}_J,
\end{aligned}
\tag{4.2}
$$

where $\hat{V} = H^1(K_R) = V$ and

$$
\begin{aligned}
\hat{\alpha}(\boldsymbol{y}, \hat{\boldsymbol{x}}) &= D\Phi(\boldsymbol{y})^{-1} D\Phi(\boldsymbol{y})^{-\top} \det D\Phi(\boldsymbol{y}) \alpha(\boldsymbol{y}, \Phi^{-1}(\boldsymbol{y})(\boldsymbol{x})),\\
\hat{\kappa}^2(\boldsymbol{y}, \hat{\boldsymbol{x}}) &= \det D\Phi(\boldsymbol{y}) \kappa^2(\boldsymbol{y}, \Phi^{-1}(\boldsymbol{y})(\boldsymbol{x})),
\end{aligned}
\tag{4.3}
$$

with $D\Phi(\boldsymbol{y})$ the Jacobian matrix of $\Phi(\boldsymbol{y})$. In (4.2), $\hat{\nabla}$ denotes the gradient with respect to $\hat{\boldsymbol{x}} \in K_R$, the coordinates in the nominal configuration.

Remark 4.1 Formulae (4.3) explain why we have to require $k \geq 1$ in Assumption 3.1 and $p < \frac{1}{2}$ in Assumption 2.4 (since in general $D\Phi$ and its inverse will depend on $\frac{\partial r}{\partial \varphi}$).

We are now in a position to give a rigorous definition for the solution to (4.1):

Definition 4.2 The function $u(\boldsymbol{y})$, $\boldsymbol{y} \in \mathcal{P}_J$, is a solution to (4.1) if and only if its pullback $(\Phi^*(\boldsymbol{y})u(\boldsymbol{y}))(\hat{\boldsymbol{x}}) := u(\Phi(\boldsymbol{y}, \hat{\boldsymbol{x}})) \in H^1(K_R)$ is a solution to (4.2).

4.2 Well-posedness of the model problem

Existence and uniqueness of the solution are ensured by the following theorem:

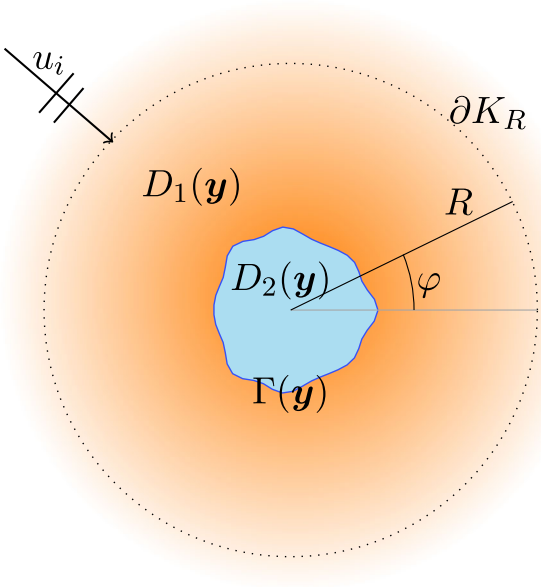

Fig. 3 Domain considered in (4.1)

Theorem 4.3 *The solution to the variational formulation* (4.1) *exists and is unique, for every* $J \in \mathbb{N}$ *and every* $\boldsymbol{y} \in \mathcal{P}_J$. *Equivalently, if Assumption 3.1 is fulfilled, then* (4.2) *admits a unique solution for every* $J \in \mathbb{N}$ *and every* $\boldsymbol{y} \in \mathcal{P}_J$.

Proof The boundedness of K_R allows us to apply the Fredholm Alternative [36, Thm. 2.27] to get existence of the solution to (4.2), while uniqueness is ensured by the sign properties of the DtN map. We refer to [42, Thm. 3.2.3] for the detailed proof. □

To have well-posedness of the problem, we still have to prove that the solution to (4.2) depends continuously on the data, which in our case consist of the incoming wave u_i. Thus, we would desire to have a bound on the $H^1(K_R)$-norm of $\hat{u}$ by some norm of u_i. This stability property will be needed later for convergence purposes (Section 5).

Unfortunately, a J- and $\boldsymbol{y}$-uniform stability result cannot be achieved in general for the Helmholtz equation. The reason being that, without any limitation on the wavenumber, it can happen that a small wavenumber excites resonances at the boundary of the scatterer, with an uncontrollable increase of the amplitude of the field u in that region. Therefore, we assume that the wavelength is large enough compared to the scatterer size:

Assumption 4.4 (Large wavelength assumption) *The wavenumbers in* (1.2) *satisfy the condition:*

$$\kappa_1^2, \kappa_2^2 \leq \tau\, C(R), \quad \textit{for some } 0 < \tau < \min\{1, \alpha_2\}, \tag{4.4}$$

with

$$C(R) = \inf_{w \in H^1(K_R)} \frac{|w|^2_{H^1(K_R)} + \|w\|^2_{L^2(\partial K_R)}}{\|w\|^2_{L^2(K_R)}}. \tag{4.5}$$

This leads to the following stability result:

Lemma 4.5 *Let Assumption 3.1 be satisfied. There exists a constant* $0 < T < 1$ *independent of* $J \in \mathbb{N}$ *and* $\boldsymbol{y} \in \mathcal{P}_J$ *such that, if Assumption 4.4 holds with* $\tau < T$*, then:*

(a) *the bilinear form* $\hat{a}_y(\cdot, \cdot)$ *in (4.2) is coercive, with coercivity constant independent of* $J \in \mathbb{N}$ *and* $\boldsymbol{y} \in \mathcal{P}_J$*;*

(b) *there exist positive constants* B_1*,* B_2 *independent of* $J \in \mathbb{N}$ *and of* $\boldsymbol{y} \in \mathcal{P}_J$ *(but which do depend on* $\alpha_2, \sigma_{min}, \sigma_{max}, \kappa_1, \kappa_2$ *and* R*) such that, for every* $J \in \mathbb{N}$ *and every* $\boldsymbol{y} \in \mathcal{P}_J$*:*

$$\left\|\hat{u}(\boldsymbol{y})\right\|_{H^1(K_R)} \leq B_1 \left\|u_i\right\|_{H^{\frac{1}{2}}(\partial K_R)} + B_2 \left\| \frac{\partial u_i}{\partial \boldsymbol{n}_R} \right\|_{H^{-\frac{1}{2}}(\partial K_R)}, \tag{4.6}$$

with $\dfrac{\partial u_i}{\partial \boldsymbol{n}_R} = \boldsymbol{d} \cdot \boldsymbol{n}_R \kappa_1 e^{i\kappa_1 \boldsymbol{d}\cdot\boldsymbol{x}}$.

Proof See Lemma 3.2.5 and Cor. 3.2.6 in [42]. □

The variational form (4.2) is now ready to be discretized. Notice that *two* discretizations are needed: the discretization in the parameter space and the space discretization on the nominal configuration. The former will be considered in Section 5, while for the latter we rely on a standard finite element discretization, of which we will provide details in Section 6.

5 Stochastic collocation and Smolyak algorithm

In this section we address the parameter space discretization of (4.2) through stochastic collocation. In the first subsection we recall the main features of sparse interpolation and quadrature. In the second subsection, we describe the sparse adaptive Smolyak algorithm used in our numerical experiments to select the collocation points. In the third and last subsection, we show that the hypothesis for the convergence theorems for the sparse interpolation and quadrature hold for the Helmholtz transmission problem.

In the first two subsections, we present the results in the general case that the parameter space is $\mathcal{P} := [-1, 1]^d$ with d large and possibly infinite (in the latter case we write $[-1, 1]^\infty = \bigotimes_{j=1}^{\infty} [-1, 1]$ for the set of infinite sequences where every term is in $[-1, 1]$). When we apply them to our model problem, we consider then $\mathcal{P}_J = [-1, 1]^{2J}$ as parameter space (i.e. $d = 2J$).

5.1 High-dimensional sparse polynomial interpolation and quadrature

We only recall the main definitions and properties used in the continuation of the paper. For an exhaustive survey on stochastic collocation, we refer to [2] and [48]. Details on sparse polynomial interpolation and sparse quadrature can be found in [9] and [43], respectively.

Univariate operators and tensorization Let $\left(\zeta_j^k\right)_{j=0}^{n_k}$ be a sequence of distinct points in $\mathcal{P}_l = [-1, 1]$ (for a generic $l \geq 1$), associated with the weights $\left(w_j^k\right)_{j=0}^{n_k}$. The univariate polynomial interpolation operator I_k and the univariate quadrature operator Q_k associated with the points $\left\{\zeta_0^k, \ldots, \zeta_{n_k}^k\right\}$ are defined as

$$I_k g = \sum_{i=0}^{n_k} g(\zeta_i^k) l_i^{n_k}, \quad Q_k g = \sum_{i=0}^{n_k} w_i^{n_k} \cdot g(\zeta_i^k) = \int_{-1}^{1} I_k g(\zeta)\, d\zeta, \tag{5.1}$$

where g is a real- or complex-valued function defined on $[-1, 1]$ and $l_i^{n_k}(y) = \prod_{\substack{j=0 \\ j\neq i}}^{n_k} \frac{y-\zeta_j}{\zeta_i-\zeta_j}$ is the Lagrange polynomial associated with the nodes $\left(\zeta_j^k\right)_{j=0}^{n_k}$.

Let $\mathcal{I}(\cdot)$ be the exact integration operator, and let us denote $\mathbb{N}_0 := \mathbb{N} \cup \{0\}$. We require:

Assumption 5.1 *For each $k \in \mathbb{N}_0$, the univariate interpolation formula I_k and the univariate quadrature formula Q_k associated with the quadrature points $\left(\zeta_j^k\right)_{j=0}^{n_k}$ satisfy:*

(i) *Q_k is of order k, i.e. $(\mathcal{I} - Q_k)(p_k) = 0$ for all $p_k \in \mathbb{P}_k$, with $\mathbb{P}_k$ the set of polynomials up to the k-th degree;*

(ii) *the Lebesgue constants λ_k of I_k and $\sum_{j=0}^{n_k} |w_j^k|$ behave like $\mathcal{O}((k+1)^\theta)$ for some $\theta \geq 1$.*

The univariate interpolation and quadrature difference operators are defined as

$$\Delta_k^I = I_k - I_{k-1}, \quad \Delta_k^Q = Q_k - Q_{k-1}, \quad k \geq 0, \tag{5.2}$$

where we set $I_{-1} = 0$, so that $\Delta_0^I g = g(\zeta_0^0)$, and $Q_{-1} = 0$, $\zeta_0^0 = 0$, $w_0^0 = 1$, so that $Q_0 g = g(0)$. Therefore, (5.1) can be rewritten as

$$I_k = \sum_{j=0}^{k} \Delta_j^I, \quad Q_k = \sum_{j=0}^{k} \Delta_j^Q. \tag{5.3}$$

We remark that any univariate family of interpolation points can be used for the above construction, in particular the sequences need not to be nested.

To extend these concepts to the multi-dimensional case, we introduce the set

$$\mathcal{F} = \left\{ \nu \in \mathbb{N}_0^{\mathbb{N}} : \sharp\, \mathrm{supp}\ \nu < \infty \right\}, \tag{5.4}$$

where the support of a multi-index is defined as $\mathrm{supp}\ \nu = \left\{ j \in \mathbb{N} : \nu_j \neq 0 \right\}$.

To any multi-index $\nu \in \mathcal{F}$, we associate the set of multivariate points $\boldsymbol{\zeta}_\nu = \bigotimes_{j\geq 1} \left(\zeta_i^{\nu_j}\right)_{i=0}^{n_{\nu_j}} \subset \mathcal{P}$ and the tensorized multivariate operators

$$I_\nu = \bigotimes_{j\geq 1} I_{\nu_j} \quad \text{and} \quad \Delta_\nu^I = \bigotimes_{j\geq 1} \Delta_{\nu_j}^I, \tag{5.5}$$

$$Q_\nu = \bigotimes_{j\geq 1} Q_{\nu_j} \quad \text{and} \quad \Delta_\nu^Q = \bigotimes_{j\geq 1} \Delta_{\nu_j}^Q. \tag{5.6}$$

We refer to [9, p.608] and [43, p.9] for a more rigorous definition, using induction, of the tensorized interpolation and quadrature operators, respectively.

Sparse interpolation and quadrature operators To define sparse interpolation and quadrature operators, we introduce the following notion:

Definition 5.2 (Definition 3.1 in [43]) A subset $\Lambda \subset \mathcal{F}$ of finite cardinality N is called downward closed[1] if $\{0\} \subset \Lambda$ and if, for every $\nu \in \Lambda$, $\nu \neq 0$, it holds that $\nu - e_j \in \Lambda$ for all $j \in \operatorname{supp} \nu$, where $e_j \in \{0,1\}^{\mathbb{N}}$ denotes the index vector with 1 in position $j \in \mathbb{N}$ and 0 in all other positions $i \in \mathbb{N} \setminus \{j\}$.

For any downward closed set $\Lambda \subset \mathcal{F}$, the sparse interpolation and quadrature operators are

$$I_\Lambda = \sum_{\nu\in\Lambda} \Delta_\nu^I, \quad Q_\Lambda = \sum_{\nu\in\Lambda} \Delta_\nu^Q, \tag{5.7}$$

with Δ_ν^I and Δ_ν^Q the multivariate difference operators defined in (5.5) and (5.6), respectively. Theorem 2.1 in [9] and Theorem 4.2 in [43] ensure that these operators are well defined.

We have introduced the definitions for the case that g is a real- or complex-valued function, but they can be extended in a straightforward way to functions taking values in separable Banach spaces, see [9] and [43] for details.

Best N-term convergence rates for sparse interpolation and quadrature For $s > 1$, we define the Bernstein ellipse in the complex plane as $\mathcal{E}_s := \left\{\frac{w+w^{-1}}{2} : 1 \leq |w| \leq s\right\}$. Given a sequence $\boldsymbol{\rho} := (\rho_l)_{l\geq 1}$, $\mathcal{E}_{\boldsymbol{\rho}} = \bigotimes_{l\geq 1} \mathcal{E}_{\rho_l}$ denotes the tensorized polyellipse [10].

Given a Q.o.I. g that, for each $\boldsymbol{y} \in \mathcal{P}$, takes values in a separable Hilbert space V, we call the map $\boldsymbol{y} \in \mathcal{P} \mapsto g(\boldsymbol{y}) \in V$ the *solution map*.

For the convergence results for the sparse interpolation and quadrature operators to hold, we need that the function that we want to interpolate or of which we want to compute the integral fulfills some regularity properties [10, 43, 44]:

$(\boldsymbol{b}, \boldsymbol{p}, \boldsymbol{\varepsilon})$-holomorphy assumption Let $g : \mathcal{P} \to V$ denote a bounded, continuous function of countably many variables $y_1, y_2, \ldots$, defined on $\mathcal{P} = [-1,1]^\infty$ and taking values in a separable Hilbert space V. We require that:

[1] Also referred to in the literature as *lower index set* or *monotone index set*.

(i) Given a positive sequence $\boldsymbol{b} = (b_l)_{l\geq 1} \in \ell^p(\mathbb{N})$ for some $0 < p < 1$, there exists a real number $0 < \varepsilon < 1$ such that, for every $(\boldsymbol{b}, \varepsilon)$-admissible sequence of poly-radii, i.e. for every sequence $\boldsymbol{\rho} = (\rho_l)_{l\geq 1}$ such that $\rho_l > 1$ and

$$\sum_{l\geq 1}(\rho_l - 1)b_l \leq \varepsilon, \tag{5.8}$$

the solution map $\boldsymbol{y} \mapsto g(\boldsymbol{y})$ admits a holomorphic extension to a set of the form $\mathcal{O}_{\boldsymbol{\rho}} := \bigotimes_{l\geq 1} \mathcal{O}_{\rho_l}$, with $\mathcal{O}_{\rho_l} \subset \mathbb{C}$ an open set containing $\mathcal{E}_{\rho_l}$, $l \geq 1$.

(ii) g satisfies an a priori estimate (uniform upper bound)

$$\sup_{z\in\mathcal{E}_{\boldsymbol{\rho}}} \|g(z)\|_V \leq B(\varepsilon), \tag{5.9}$$

for a constant $B = B(\varepsilon)$ independent of $\boldsymbol{\rho}$ and the dimension of the parameter space.

Lemma 4.4 in [10] ensures that, for $s > 1$, the open set $\mathcal{O}_s := \{z \in \mathbb{C} : \mathrm{dist}(z, [-1, 1]) < s - 1\}$ is an open neighborhood of $\mathcal{E}_s$. Then, it is sufficient to verify the $(\boldsymbol{b}, p, \varepsilon)$-holomorphy assumption on sets of the form

$$\mathcal{O}_{\boldsymbol{\rho}} = \bigotimes_{l\geq 1} \mathcal{O}_{\rho_l}, \quad \text{with } \mathcal{O}_{\rho_l} = \{z \in \mathbb{C} : \mathrm{dist}(z, [-1, 1]) < \rho_l - 1\}, \ l \geq 1. \tag{5.10}$$

Under the $(\boldsymbol{b}, p, \varepsilon)$-holomorphy assumption, one can prove the following convergence results:

Theorem 5.3 *(Theorem 4.4 in [9]) Let the $(\boldsymbol{b}, p, \varepsilon)$-holomorphy assumption be satisfied. If the univariate sequence $\left(\zeta_j^k\right)_{j=0}^{n_k}$ is chosen so that Assumption 5.1 (ii) is fulfilled, then there exists a sequence $(\Lambda_N)_{N\geq 1}$ of downward closed sets $\Lambda_N \subset \mathcal{F}$ such that $\sharp\Lambda_N = N$ and*

$$\|g - I_{\Lambda} g\|_{L^\infty(\mathcal{P},V)} \leq CN^{-s}, \quad s = \frac{1}{p} - 1. \tag{5.11}$$

Theorem 5.4 *(Lemma 4.10 in [43]) Let the $(\boldsymbol{b}, p, \varepsilon)$-holomorphy assumption and Assumption 5.1 be satisfied. Then there exists a sequence $(\Lambda_N)_{N\geq 1}$ of downward closed sets $\Lambda_N \subset \mathcal{F}$ such that $\sharp\Lambda_N \leq N$ and*

$$\|\mathcal{I}(g) - Q_{\Lambda} g\|_V \leq CN^{-s}, \quad s = \frac{1}{p} - 1. \tag{5.12}$$

These two results show convergence rates which depend only on p, referred to as the 'sparsity class of the unknown', while they do not depend on the number of dimensions activated. This means that we can break the curse of dimensionality by algorithms which adaptively construct downward closed index sets for the sparse interpolation and quadrature operators, as the algorithm that we present in the next subsection.

Remark 5.5 Recent advances in [50] show that, for symmetric probability measures (as the uniform measure used in the present paper), the convergence rate for the sparse

quadrature operator can be improved to $\frac{2}{p} - 1$. However, numerical experiments in [50] show that, when the deviation of the integrand around the mean is not small, a long preasymptotic phase prevents us from observing the improved rate unless an extremely large number of quadrature points is used.

5.2 The sparse adaptive Smolyak algorithm

The idea is to identify the index set Λ_N of the N indices in $\mathcal{F}$ giving the highest contribution to the approximations (5.7). However, the index set Λ_N built in this way would be nested but not downward closed and, even worse, the cardinality of the set that should be considered to update Λ_N at each step grows exponentially with the number of dimensions activated and it would be infinite in the case of countably many parameters. To overcome this, one considers a local subset of $\mathcal{F}$, referred to as the *reduced set of neighbors* of a given finite set $\Lambda \subset \mathcal{F}$, specifically [23]:

$$\mathcal{N}(\Lambda) = \left\{\nu \notin \Lambda : \nu - e_j \in \Lambda, \text{ for all } j \in \operatorname{supp} \nu \text{ and } \nu_j = 0, \text{ all } j > j(\Lambda) + 1\right\} \tag{5.13}$$

for any downward closed index set Λ, where $j(\Lambda) = \max\left\{j : \nu_j > 0 \text{ for some } \nu \in \Lambda\right\}$. Using this set of neighbors, at each iteration at most one additional dimension can be activated.

The algorithm constructs then an anisotropic downward closed index set Λ comprising those indices in $\mathcal{N}(\Lambda)$ which are expected to contribute most to the approximation (see [43] for details):

Algorithm 1 Sparse adaptive Smolyak algorithm

1: **function** ASG
2: Set $\Lambda_1 = \{0_{\mathcal{F}}\}$, $k = 1$ and compute $\Delta_0^Q(g)$.
3: Determine the reduced set of neighbors $\mathcal{N}(\Lambda_1)$.
4: Compute $\Delta_\nu^Q(g)$, for all $\nu \in \mathcal{N}(\Lambda_1)$.
5: **while** $\sum_{\nu\in\mathcal{N}(\Lambda_k)} \|\Delta_\nu^Q(g)\|_V > tol$ **do**
6: Set $\Lambda_{k+1} = \Lambda_k \cup \left\{\mu \in \mathcal{N}(\Lambda_k) : \|\Delta_\mu^Q(g)\|_V \geq \vartheta \max_{\nu\in\mathcal{N}_{\Lambda_k}} \|\Delta_\nu^Q(g)\|_V\right\}$.
7: Determine the reduced set of neighbors $\mathcal{N}(\Lambda_{k+1})$.
8: Compute $\Delta_\nu^Q(g)$, for all $\nu \in \mathcal{N}(\Lambda_{k+1})$.
9: Set $k = k + 1$.
10: **end while**
11: **end function**

In line 6, $\vartheta \in [0, 1]$ is a parameter chosen at the beginning of the algorithm, and determining how many indices in the reduced set of neighbors are included in the set Λ at each iteration. For $\theta = 1$, we have $\Lambda_{k+1} = \Lambda_k \cup \{\bar{\nu}\}$ with $\bar{\nu} = \operatorname{argmax}_{\nu\in\mathcal{N}_\Lambda} \|\Delta_\nu^Q(g)\|_V$.

For the interpolation, the difference operators are the ones defined in (5.5). For each $\nu \in \mathcal{F}$, $\|\Delta_\nu^Q(g)\|_V$ is replaced by $\|\Delta_\nu^I(g)\|_{L^\infty(\mathcal{P},V)}$, and the stopping criterion $\sum_{\nu\in\mathcal{N}(\Lambda_k)} \|\Delta_\nu^Q(g)\|_V \leq tol$ at line 5 of Algorithm 1 is substituted by the condition $\max_{\nu\in\mathcal{N}(\Lambda_k)} \|\Delta_\nu^I(g)\|_V \leq tol$.

Remark 5.6 We remark that there is no guarantee and it has not been proved that the downward closed index sets obtained with Algorithm 1 are the ones for which the estimates in Theorems 5.3 and 5.4 hold, and it could be possible to encounter cases where no convergence can be observed. However, in [43] several numerical examples are shown where the convergence rates of Theorems 5.3 and 5.4 are achieved. Also our numerical experiments of Section 7 will confirm that the proposed algorithm remains effective in all test cases.

5.3 Analyticity and uniform boundedness of solutions to elliptic PDEs

Let us now return to our model problem as stated in (4.2). We need to show that this case satisfies the $(\boldsymbol{b}, p, \varepsilon)$-holomorphy assumption, so that the convergence results stated in Theorems 5.3 and 5.4 hold.

To this aim, we replace the definition of $(\boldsymbol{b}, \varepsilon)$-admissible sequence of polyradii by the following:

Definition 5.7 A sequence $\boldsymbol{\rho} = (\rho_l)_{l\geq 1}$ of polyradii, with $\rho_l > 1$ for every $l \in \mathbb{N}$, is said to be $(\boldsymbol{b}, \varepsilon)^*$-admissible if it is $(\boldsymbol{b}, \varepsilon)$-admissible for a sequence $\boldsymbol{b}$ that has a *monotonic* majorant in $\ell^p(\mathcal{F})$ for $0 < p < \frac{1}{2}$ and is such that $(lb_l^p)_{l\geq 1}$ has a monotonic majorant, and if (5.8) is replaced by

$$\sum_{l\geq 1}(\rho_l - 1)lb_l \leq \varepsilon. \tag{5.14}$$

We use the term $(\boldsymbol{b}, p, \varepsilon)^*$-holomorphy assumption to denote the $(\boldsymbol{b}, p, \varepsilon)$-holomorphy assumption when $(\boldsymbol{b}, \varepsilon)$-admissible sequences are replaced by $(\boldsymbol{b}, \varepsilon)^*$-admissible sequences.

Proposition 5.8 *Let the $(\boldsymbol{b}, p, \varepsilon)$-assumption be replaced by the $(\boldsymbol{b}, p, \varepsilon)^*$-assumption. Then the algebraic convergence of the sparse interpolation and quadrature operators, prescribed by Theorems 5.3 and 5.4 respectively, still holds with rate of convergence $s = \frac{1}{p} - 2$.*

Proof Since the sequence $\boldsymbol{b}$ has a monotonic majorant in $\ell^p(\mathcal{F})$ and the sequence $(lb_l^p)_{l\geq 1}$ has a monotonic majorant, Lemma C.0.7 in [42] ensures that the sequence $(lb_l)_{l\geq 1}$ belongs to $\ell^q(\mathcal{F})$ with $q = \frac{p}{1-p}$. Applying Theorems 5.3 and 5.4 using the $(\boldsymbol{b}, p, \varepsilon)$-assumption for the sequence $\tilde{\boldsymbol{b}} = (lb_l)_{l\geq 1}$, we obtain the claim. □

Remark 5.9 The condition expressed by the inequality in (5.14), differently from the condition $\boldsymbol{b} \in \ell^p(\mathbb{N})$, entails an implicit ordering of the dimensions of the

parameter space with respect to decreasing significance. However, thanks to Assumption 2.4, the bound ε in (5.14) does not depend on the sequence $\boldsymbol{b}$ itself but on its (monotonically decreasing) majorant.

Remark 5.10 Condition (5.14) implies in particular condition (5.8) for the same sequence $\boldsymbol{b}$.

Our plan is to show that the $(\boldsymbol{b}, p, \varepsilon)^*$-holomorphy assumption is fulfilled for our model problem.

As it is done in [10, Sect. 5.3], we choose the sequence $\boldsymbol{b}$ as

$$b_l = \|\beta_l \psi_l\|_{C^0_{\mathrm{per}}([0,2\pi))} + \left\|\beta_l \psi_l'\right\|_{C^0_{\mathrm{per}}([0,2\pi))} = |\beta_l| + l|\beta_l|, \quad l \geq 1, \tag{5.15}$$

with β_l and ψ_l as in Remark 2.6, $l \geq 1$. Notice that, thanks to Assumption 2.4 on the sequence $(\beta_l)_{l\geq 1}$ (i.e. existence of a monotonic majorant belonging to $\ell^p(\mathbb{N})$ with $p < \frac{1}{2}$), there exist sequences of polyradii that are $(\boldsymbol{b}, \varepsilon)^*$-admissible.

We show explicitly that the $(\boldsymbol{b}, \varepsilon)^*$-holomorphy assumption is fulfilled when using the domain mapping (3.2). However, our results hold for a generic mapping fulfilling the following conditions, slightly stronger than the ones in Assumption 3.1:

Assumption 5.11 *(i) The domain mapping $\Phi = \Phi(\boldsymbol{y})$, its Jacobian matrix $D\Phi(\boldsymbol{y})$ and its inverse $D\Phi^{-1}(\boldsymbol{y})$, $\boldsymbol{y} \in \mathcal{P}_J$, $J \in \mathbb{N}$, admit a holomorphic extension to the subsets $\mathcal{O}_{\boldsymbol{\rho}} \subset \mathbb{C}^{\mathbb{N}}$ as defined in (5.10), for any $(\boldsymbol{b}, \varepsilon)^*$-admissible sequence of polyradii $\boldsymbol{\rho}$.*

(ii) For every $\boldsymbol{z} \in \mathcal{O}_{\boldsymbol{\rho}}$, $\Phi = \Phi(\boldsymbol{z})$ fulfills Assumption 3.1, with bounds possibly depending on ε. For Assumption 3.1(i), the requirement on the diffeomorphism to be orientation-preserving is replaced by: there exists a real constant $\sigma_- = \sigma(\varepsilon) > 0$ independent of $\boldsymbol{z} \in \mathcal{O}_{\boldsymbol{\rho}}$ such that

$$\operatorname{Re} \det D\Phi(\boldsymbol{z}) > \sigma(\varepsilon) \quad \text{for every } \boldsymbol{z} \in \mathcal{O}_{\boldsymbol{\rho}}. \tag{5.16}$$

Let us first look at the uniform bound (5.9).

Assumption 2.3 ensures that there exist $0 < r^-, r^+ < \infty$ such that

$$r^- \leq r(\boldsymbol{y}, \varphi) \leq r^+ \quad \text{for a.e. } \varphi \in [0, 2\pi), \text{ all } J \in \mathbb{N}, \text{ and all } \boldsymbol{y} \in \mathcal{P}_J \tag{5.17}$$

(more precisely, in our case $r^- = \frac{r_0^-}{2}$, $r^+ = r_0^+ + \frac{r_0^-}{2}$, with $r_0^+ = \sup_{\varphi\in[0,2\pi)} r_0(\varphi)$ and r_0^- as in Assumption 2.3). Moreover, Assumption 2.4 guarantees (see e.g. [42, Lemma C.0.5]) that there exists a J- and $\boldsymbol{y}$- independent constant $0 < C_r < \infty$ such that

$$\left\|\frac{\partial r}{\partial \varphi}(\boldsymbol{y})\right\|_{C^0_{\mathrm{per}}([0,2\pi))} \leq \left\|\frac{\partial r_0}{\partial \varphi}\right\|_{C^0_{\mathrm{per}}([0,2\pi))} + C_r \quad \text{for all } J \in \mathbb{N} \text{ and all } \boldsymbol{y} \in \mathcal{P}_J. \tag{5.18}$$

Using these facts, we can prove the following:

Lemma 5.12 *Let $\boldsymbol{b}$ be as in (5.15) and $0 < \varepsilon < \frac{r^-}{2}$, with r^- as in (5.17). Then, for every $(\boldsymbol{b}, \varepsilon)^*$-admissible sequence $\boldsymbol{\rho}$ and every $\boldsymbol{z} \in \mathcal{O}_{\boldsymbol{\rho}}$, with $\mathcal{O}_{\boldsymbol{\rho}}$ as in (5.10), we*

have the z-independent bounds

$$\frac{r^-}{2} \leq \operatorname{Re} r(z,\varphi), \qquad \varphi \in [0,2\pi), \tag{5.19}$$

$$\frac{r^-}{2} \leq |r(z,\varphi)| \leq r^+ + \varepsilon, \qquad \varphi \in [0,2\pi), \tag{5.20}$$

$$\left|\frac{\partial r}{\partial \varphi}(z,\varphi)\right| \leq \left\|\frac{\partial r_0}{\partial \varphi}\right\|_{C^0_{per}([0,2\pi))} + C_r + \varepsilon, \qquad \varphi \in [0,2\pi), \tag{5.21}$$

with r^+ as in (5.17) and C_r as in (5.18).

In particular, the mapping Φ defined in (3.2) fulfills Assumption 5.11 (ii) if the mollifier fulfills Assumption 3.3 and $0 < \varepsilon < \min\left\{c_\chi, \frac{r^-}{2}\right\}$.

Proof The results follow immediately from the bounds (5.17) and (5.18). We refer to Lemma 4.3.6 in [42] for the complete proof. □

The same argument used in the proof of Lemma 4.5 leads to:

Proposition 5.13 *Let the sequence $\boldsymbol{b}$ be as in (5.15) and $0 < \varepsilon < \frac{r^-}{2}$, with r^- as in (5.17).*

If the mapping Φ satisfies Assumption 5.11, then part (ii) of the $(\boldsymbol{b}, p, \varepsilon)^*$-holomorphy assumption is fulfilled, i.e. there exist constants $B_1 = B_1(\varepsilon)$ and $B_2 = B_2(\varepsilon)$ such that

$$\sup_{z\in\mathcal{O}_{\boldsymbol{\rho}}} \left\|\hat{u}(z)\right\|_{H^1(K_R)} \leq B_1(\varepsilon)\left\|u_i\right\|_{H^1(\partial K_R)} + B_2(\varepsilon)\left\|\frac{\partial u_i}{\partial \boldsymbol{n}_R}\right\|_{L^2(\partial K_R)} \tag{5.22}$$

for every $\mathcal{O}_{\boldsymbol{\rho}}$, with $\mathcal{O}_{\boldsymbol{\rho}}$ as in (5.10) and $\boldsymbol{\rho}$ any sequence of $(\boldsymbol{b}, \varepsilon)^*$-admissible polyradii. The constants B_1 and B_2 are independent of $J \in \mathbb{N}$, $\boldsymbol{y} \in \mathcal{P}_J$ and $\boldsymbol{\rho}$.

In particular, the bound (5.22) holds for the mapping Φ given in (3.2) if the mollifier fulfills Assumption 3.3 and $0 < \varepsilon < \min\left\{c_\chi, \frac{r^-}{2}\right\}$.

To prove that part (i) of the $(\boldsymbol{b}, p, \varepsilon)^*$-holomorphy assumption holds, we first show the existence of a holomorphic extension for the parameter-dependent radius (2.6) and its φ-derivative; from this, analyticity of the map $\Phi(\boldsymbol{y})$ and then of the solution to the PDE on the nominal configuration follow. The proof is rather general and actually it applies, with minor modifications, to any elliptic PDE as long as the parameter-dependent configuration can be mapped to a reference configuration through a mapping satisfying Assumption 5.11 and depending smoothly on the stochastic quantity $r = r(\boldsymbol{y})$.

Lemma 5.14 *For every $z \in \mathcal{O}_{\boldsymbol{\rho}}$, with $\mathcal{O}_{\boldsymbol{\rho}}$ as in (5.10) and $\boldsymbol{\rho}$ any $(\boldsymbol{b}, \varepsilon)^*$-admissible sequence, the maps $z \mapsto r(z) \in C^1_{per}([0,2\pi))$ and $z \mapsto \frac{\partial r}{\partial \varphi}(z) \in C^0_{per}([0,2\pi))$, with $r = r(z)$ given by (2.6), are holomorphic.*

Proof The result follows immediately from Hartogs' theorem on separate analyticity and the bounds (5.8), (5.14) on the sequence $\boldsymbol{b}$. □

Let $\mathrm{Diff}^k_{+,\hat{pw}}(K_R, K_R)$ be the space of diffeomorphisms which are of order C^k in each of the two subdomains $\overline{\hat{D}_1 \cap K_R}$ and $\overline{\hat{D}_2}$, and with determinant with positive real part. Since algebraic sum, multiplication and division by holomorphic functions which are not zero is still holomorphic, it follows immediately from Lemma 5.14 that:

Lemma 5.15 *Let us consider the map Φ defined in (3.2) with mollifier fulfilling Assumption 3.3. Then the mappings $z \mapsto \Phi(z,\cdot) \in Diff^1_{+,pw}(K_R, K_R)$ and $z \mapsto \det D\Phi(z,\cdot) \in C^0_{pw}(\overline{K_R})$ are holomorphic in $\mathcal{O}_{\boldsymbol{\rho}}$, with $\mathcal{O}_{\boldsymbol{\rho}}$ as defined in (5.10) for any $(\boldsymbol{b},\varepsilon)^*$-admissible sequence $\boldsymbol{\rho}$.*

Together with Lemma 5.12, this implies that the mapping defined in (3.2) (with Assumption 3.3 on the mollifier) satisfies Assumption 5.11.

Proof It is easy to check that, thanks to Assumption 2.3 and the restrictions on the mollifier χ, the denominators in the entries of $D\Phi(z)$ and $D\Phi^{-1}(z)$ are never zero, for every $z \in \mathcal{O}_{\boldsymbol{\rho}}$. Thus $z \mapsto \Phi(z)$, $z \mapsto D\Phi(z)$ and $z \mapsto D\Phi^{-1}(z)$ are holomorphic. □

For the same reasons as for the previous lemma, we also have:

Lemma 5.16 *Let Assumption 5.11 be fulfilled. Then the coefficients $\hat{\alpha}(\boldsymbol{y})$, $\hat{\kappa}^2(\boldsymbol{y})$ as defined in (4.3) are holomorphic when considered as maps from $\boldsymbol{z} \in \mathcal{O}_{\boldsymbol{\rho}}$ to $C^0_{\hat{pw}}(\overline{K_R})$.*

This implies immediately:

Lemma 5.17 *Let Assumptions 4.4 and 5.11 hold, the former with $\tau < T$ and T as in Lemma 4.5. Then, if $\hat{u}$ is a solution to (4.2), the solution map $\boldsymbol{y} \mapsto \hat{u}(\boldsymbol{y})$, admits a holomorphic extension to any open set $\mathcal{O}_{\boldsymbol{\rho}} \subset \mathbb{C}^{\mathbb{N}}$ as defined in (5.10), with $\boldsymbol{\rho}$ a $(\boldsymbol{b},\varepsilon)^*$-admissible sequence.*

For each variable z_l, $l \geq 1$, the complex derivative $\left(\partial_{z_l}\hat{u}\right)(z) \in V$ is the weak solution to the variational problem:

$$\text{Find } \left(\partial_{z_l}\hat{u}\right)(z) \in V :$$

$$\int_{K_R} \left(\hat{\alpha}(z,\hat{\boldsymbol{x}})\hat{\nabla}\partial_{z_l}\hat{u}(z,\hat{\boldsymbol{x}}) \cdot \hat{\nabla}\hat{v}(\hat{\boldsymbol{x}}) - \hat{\kappa}^2(z,\hat{\boldsymbol{x}})\partial_{z_l}\hat{u}(z,\hat{\boldsymbol{x}})\hat{v}(\hat{\boldsymbol{x}})\right) d\hat{\boldsymbol{x}}$$

$$- \int_{\partial K_R} DtN(\partial_{z_l}\hat{u}(z,\hat{\boldsymbol{x}}))\hat{v}(\hat{\boldsymbol{x}})\, dS = L_0(z,\hat{v}) \quad \text{for all } \hat{v} \in V \text{ and all } z \in \mathcal{O}_{\boldsymbol{\rho}}. \tag{5.23}$$

The right-hand side L_0 is given by

$$L_0(z,\hat{v}) = \int_{K_R} -\frac{\partial\hat{\alpha}}{\partial z_l}(z,\hat{\boldsymbol{x}})\hat{\nabla}\hat{u}(z,\hat{\boldsymbol{x}}) \cdot \hat{\nabla}\hat{v}(\hat{\boldsymbol{x}})\, d\hat{\boldsymbol{x}} + \frac{\partial\hat{\kappa}^2}{\partial z_l}(z,\hat{\boldsymbol{x}})\hat{u}(z,\hat{\boldsymbol{x}})\hat{v}(\hat{\boldsymbol{x}})\, d\hat{\boldsymbol{x}}.$$

In particular, this result holds when using the domain mapping defined in (3.2) with the mollifier fulfilling Assumption 3.3.

Proof Lemma 5.16 shows that the bilinear form in (4.2), with $\boldsymbol{y} \in \mathcal{P}_J$, $J \in \mathbb{N}$, replaced by $\boldsymbol{z} \in \mathcal{O}_{\boldsymbol{\rho}}$, is holomorphic in $\mathcal{O}_{\boldsymbol{\rho}}$. The right-hand side in (4.2) does not depend on the stochastic parameter, so in this particular case we do not have to show its analyticity. Then, the result follows from Theorem 4.1 in [10]. □

Remark 5.18 The use of Theorem 4.1 in [10] in the above proof, makes the result of Lemma 5.17 easily generalizable to any elliptic PDE with analytic data.

We summarize the results obtained so far in the following proposition:

Proposition 5.19 *Let the parameter-dependent radius $r(\boldsymbol{y})$ characterizing a star-shaped stochastic interface be given by the expansion (2.6) and let Assumptions 2.2, 2.3, 2.4 and 4.4 hold. If the map $\Phi(\boldsymbol{y}) : K_R \to K_R$ satisfies Assumption 5.11, then the solution $\hat{u}$ to (4.2) is holomorphic in every $\mathcal{O}_{\boldsymbol{\rho}}$ as defined in (5.10), with $\boldsymbol{\rho}$ a $(\boldsymbol{b}, \varepsilon)^*$-admissible sequence of polyradii and $0 < \varepsilon < \frac{r^-}{2}$. In particular, if the mapping is given by (3.2) with the mollifier fulfilling Assumption 3.3, then the solution $\hat{u}$ to (4.2) is holomorphic in every $\mathcal{O}_{\boldsymbol{\rho}}$ with $\boldsymbol{\rho}$ a $(\boldsymbol{b}, \varepsilon)^*$-admissible sequence and $0 < \varepsilon < \min\left\{c_\chi, \frac{r^-}{2}\right\}$.*

Propositions 5.13 and 5.19 together give finally:

Theorem 5.20 *Let Assumptions 2.2, 2.3, 2.4 and 4.4 be satisfied. Then the $(\boldsymbol{b}, p, \varepsilon)^*$-holomorphy assumption is fulfilled for the domain mapping (3.2) with mollifier fulfilling Assumption 3.3, and the convergence rates given by Theorems 5.3 and 5.4 are achieved with $s = \frac{1}{p} - 2$.*

For a generic domain mapping, the $(\boldsymbol{b}, p, \varepsilon)^*$-holomorphy assumption is satisfied and the convergence rates of Theorems 5.3 and 5.4 are achieved with $s = \frac{1}{p} - 2$ if the map fulfills Assumption 5.11.

Remark 5.21 It is clear from our treatment that the above result can be easily extended when for the mapping (3.2) we use the mollifier (3.3).

6 Spatial regularity and convergence of the finite element solution

We first establish the relationship between the order of summability p of the coefficient sequences $\mathcal{C} = (c_j)_{j\geq 1}$, $\mathcal{S} = (s_j)_{j\geq 1}$ in (2.6) and the regularity of the solution to (4.2) for a single parameter realization (Section 6.1). This information is then used to get the order of convergence of the finite element solution and couple it to the convergence results for sparse interpolation and quadrature in the parameter space, so that in the end we get convergence estimates for the fully discretized solution. The latter estimates are first obtained in the simpler case that the same finite element discretization is used for all realizations (Section 6.2.1). Then, a more refined estimate is obtained for the case that the spatial discretization is different for each interpolation / quadrature point (Section 6.2.2), although these results are restricted

to nested sequences of points in the parameter space. Finally (Section 6.3), the above convergence results are extended for linear output functionals as Q.o.I.s.

6.1 Spatial regularity of the parametric solution

In Lemma 2.5 we have shown how the summability of the coefficient sequences $\mathcal{C} = (c_j)_{j\geq 1}$ and $\mathcal{S} = (s_j)_{j\geq 1}$ relates to the smoothness of the radius $r = r(\boldsymbol{y}, \varphi)$ given by (2.6), for every $J \in \mathbb{N}$ and every $\boldsymbol{y} \in \mathcal{P}_J$. In Lemma 3.4, we have then seen that the smoothness of the radius turns into smoothness of the mapping (3.2) for the particle in free space case.

Starting from these results, in this section we state how the summability of the coefficient sequences $\mathcal{C} = (c_j)_{j\geq 1}$ and $\mathcal{S} = (s_j)_{j\geq 1}$ turns in the end into spatial smoothness of the solution to (4.2) for every parameter realization.

It is important to highlight that, in view of the convergence estimates, we need norm bounds which are independent of the truncation dimension $J \in \mathbb{N}$ in the radius expansion.

The theorem implying smoothness of the solution to a PDE from the smoothness of the coefficients requires the latter to have essentially bounded derivatives. It turns out that the proper spaces in which to state regularity are the Sobolev spaces $W^{k,\infty}$ of functions with essentially bounded weak derivatives up to the k-th order. However, since we do not want to distinguish between weak and strong measurability of the coefficient maps $\omega \mapsto \hat{\alpha}(\omega)$, $\omega \mapsto \hat{\kappa}(\omega)$, and, thus, of the solution map $\omega \mapsto \hat{u}(\omega)$, we prefer to work in separable Banach spaces, stating the regularity results in the spaces of piecewise-C^k functions.

From Lemma 2.5 and Lemma 3.4 it follows immediately:

Lemma 6.1 *Let Assumption 2.4 hold and let the map $\Phi : \mathcal{P}_J \times K_R \to \mathcal{P}_J \times K_R$ satisfy Assumption 3.1.*

Then, for every $r(\boldsymbol{y})$ given by (2.6), every $J \in \mathbb{N}$ and every $\boldsymbol{y} \in \mathcal{P}_J$, the coefficients $\hat{\alpha}$ and $\hat{\kappa}^2$ in (4.2) satisfy

$$\|\hat{\alpha}(\boldsymbol{y})\|_{C^{k-1}_{\hat{pw}}(\overline{K_R})} \leq C_1(\mathcal{C}, \mathcal{S}), \quad \|\hat{\kappa}^2(\boldsymbol{y})\|_{C^{k-1}_{\hat{pw}}(\overline{K_R})} \leq C_2(\mathcal{C}, \mathcal{S}),$$

with $\|\cdot\|_{C^{k-1}_{\hat{pw}}(\overline{K_R})} := \|\cdot\|_{C^{k-1}(\overline{\hat{D}_1 \cap K_R}) \cup C^{k-1}(\overline{\hat{D}_2})}$, under the additional hypothesis that the nominal radius r_0 belongs to $C^k_{per}([0, 2\pi))$. The constants C_1 and C_2 depend on the regularity parameter k and on the coefficient sequences $\mathcal{C} = (c_j)_{j\geq 1}$, $\mathcal{S} = (s_j)_{j\geq 1}$, but they are independent of the truncation dimension $J \in \mathbb{N}$ and of $\boldsymbol{y} \in \mathcal{P}_J$. The regularity parameter k is the same as in Lemma 2.5:

$$k = \begin{cases} \left\lfloor \frac{1}{p} - 1 \right\rfloor & \text{if } \frac{1}{p} - 1 \text{ is not an integer,} \\ \frac{1}{p} - 2 & \text{otherwise.} \end{cases}$$

Corollary 6.2 *Under Assumption 2.4, the result of Lemma 6.1 holds for the mapping 3.2 if the mollifier fulfills Assumption 3.3.*

To state the space regularity of the solution, we proceed in three steps: local interior regularity, local regularity at the interface $\hat{\Gamma}$ and at the boundary ∂K_R, and global regularity. Here we confine ourselves to the Helmholtz transmission problem, referring to [42, Sect. 6.1] for a more general treatment, valid for any strongly elliptic equation.

The local interior regularity is a consequence of Theorem 8.10 in [25]:

Theorem 6.3 *Let Assumptions 2.3, 2.4 hold, let the nominal radius r_0 belong to $C^k_{per}([0, 2\pi))$, and let the map $\Phi : \mathcal{P}_J \times K_R \to \mathcal{P}_J \times K_R$ fulfill Assumption 3.1, with k as in Lemma 2.5. If $k \geq 2$, then, for any subdomain D' such that $\overline{D'} \subset K_R \cap \hat{D}_1$ or $\overline{D'} \subset \hat{D}_2$, the solution $\hat{u}(\boldsymbol{y})$ to (4.2) belongs to $H^k(D')$ and satisfies*

$$\|\hat{u}(\boldsymbol{y})\|_{H^k(D')} \leq C \|\hat{u}(\boldsymbol{y})\|_{H^1(K_R)}, \tag{6.1}$$

for $C = C(a_-, \mathcal{K}, d', k, |\hat{D}_1 \cap K_R|, |\hat{D}_2|)$, where $|\hat{D}_1 \cap K_R|$ and $|\hat{D}_2|$ denote the sizes of the two subdomains, $d' = \min\left\{dist(D', \partial K_R), dist(D', \hat{\Gamma})\right\}$ and

$$\mathcal{K} = \max\left\{ \sup_{\boldsymbol{y}\in\mathcal{P}_J, J\in\mathbb{N}} \|\hat{\alpha}(\boldsymbol{y})\|_{C^{k-1}_{\hat{pw}}(\overline{K_R})}, \sup_{\boldsymbol{y}\in\mathcal{P}_J, J\in\mathbb{N}} \|\hat{\kappa}^2(\boldsymbol{y})\|_{C^{k-2}_{\hat{pw}}(\overline{K_R})} \right\}.$$

The symbol a_- denotes the uniform coercivity constant as in Lemma 4.5 (a), depending on the lower and upper singular value bounds $\sigma_{min}, \sigma_{max}$ for $D\Phi^{-1}(\boldsymbol{y})$ as from Lemma 3.2. In (6.1) we have denoted $C^{k-1}_{\hat{pw}}(\overline{K_R}) = C^{k-1}\left(\overline{K_R \cap \hat{D}_1}\right) \cup C^{k-1}\left(\overline{\hat{D}_2}\right)$ and similarly for $C^{k-2}_{\hat{pw}}(\overline{K_R})$.

Furthermore, if Assumption 4.4 holds, then we have a J- and $\boldsymbol{y}$-independent bound:

$$\|\hat{u}(\boldsymbol{y})\|_{H^k(D')} \leq \tilde{C}\left(\|u_i\|_{H^{\frac{1}{2}}(\partial K_R)} + \left\| \frac{\partial u_i}{\partial \boldsymbol{n}_R} \right\|_{H^{-\frac{1}{2}}(\partial K_R)} \right), \tag{6.2}$$

with $\tilde{C} = \tilde{C}(R, a_-, \mathcal{K}, d', k, |\hat{D}_1 \cap K_R|, |\hat{D}_2|)$.

Proof One can verify that, in Theorem 8.10 in [25], if the lower bound on the coercivity constant and the upper bounds on the PDE coefficients and right-hand side are independent of $J \in \mathbb{N}$ and $\boldsymbol{y} \in \mathcal{P}_J$, then the upper bound on $\|\hat{u}(\boldsymbol{y})\|_{H^k(D')}$ is also uniform in $J \in \mathbb{N}$ and $\boldsymbol{y} \in \mathcal{P}_J$. In the case of equation (4.2), the lower bound on the coercivity constant is given by Lemma 4.5 (a), the upper bounds on the coefficients are ensured by Lemma 6.1, and the right-hand side is independent of $J \in \mathbb{N}$ and $\boldsymbol{y} \in \mathcal{P}_J$.

If Assumption 4.4 holds, then we can use (4.6) to bound $\|\hat{u}(\boldsymbol{y})\|_{H^1(K_R)}$, obtaining (6.2). □

The local regularity at the interface $\hat{\Gamma}$ and at ∂K_R follows from Theorem 4.20 in [36]:

Theorem 6.4 *Let Assumptions 2.3 and 2.4 hold, let the nominal radius r_0 belong to $C^k_{per}([0, 2\pi))$ and the map $\Phi : \mathcal{P}_J \times K_R \to \mathcal{P}_J \times K_R$ fulfill Assumption 3.1, with k*

as in Lemma 2.5. Moreover, let the interfaces $\hat{\Gamma}$ and ∂K_R be $C^{k-1,1}$. If k as in Lemma 2.5 is such that $k \geq 2$, then:

- *for any subdomain $D' \subsetneq K_R$ intersecting $\hat{\Gamma}$ (but not ∂K_R), the solution $\hat{u}(\boldsymbol{y})$ to (4.2) belongs to $H^k(D' \cap \hat{D}_1) \cup H^k(D' \cap \hat{D}_2)$ and satisfies*

$$\|\hat{u}(\boldsymbol{y})\|_{H^k(D'\cap\hat{D}_1)\cup H^k(D'\cap\hat{D}_2)} \leq C\|\hat{u}(\boldsymbol{y})\|_{H^1(K_R\cap\hat{D}_1)\cup H^1(\hat{D}_2)}, \tag{6.3}$$

  where $C = C(a_-, \mathcal{K}, d', k, |K_R|)$ with $d' = dist(D', \partial K_R)$ and the other constants defined as in Theorem 6.3;
- *for any open set D' intersecting ∂K_R (but not $\hat{\Gamma}$), the solution $\hat{u}(\boldsymbol{y})$ to (4.2) satisfies*

$$\begin{aligned}\|\hat{u}(\boldsymbol{y})\|_{H^k(\hat{D}'\cap K_R)} \leq\ & C\|\hat{u}(\boldsymbol{y})\|_{H^1(\hat{D}'\cap K_R)} \\ & + C\left(\|u_i\|_{H^{k-\frac{1}{2}}(\partial K_R)} + \left\|\frac{\partial u_i}{\partial \boldsymbol{n}_R}\right\|_{H^{k-\frac{3}{2}}(\partial K_R)}\right),\end{aligned}$$

  where $C = C(a_-, \mathcal{K}, d', k, |K_R|)$ with $d' = dist(D', \hat{\Gamma})$ and the other constants defined as in Theorem 6.3.

Furthermore, if Assumption 4.4 holds, then in both cases we have bounds on the norms which are independent of the truncation dimension $J \in \mathbb{N}$ and of $\boldsymbol{y} \in \mathcal{P}_J$:

$$\begin{aligned}\|\hat{u}(\boldsymbol{y})\|_{H^k(D'\cap\hat{D}_1)} + \|\hat{u}(\boldsymbol{y})\|_{H^k(D'\cap\hat{D}_2)} &\leq \tilde{C}_1\left(\|u_i\|_{H^{\frac{1}{2}}(\partial K_R)} + \left\|\frac{\partial u_i}{\partial \boldsymbol{n}_R}\right\|_{H^{-\frac{1}{2}}(\partial K_R)}\right), \\ \|\hat{u}(\boldsymbol{y})\|_{H^k(D'\cap K_R)} &\leq \tilde{C}_2\left(\|u_i\|_{H^{k-\frac{1}{2}}(\partial K_R)} + \left\|\frac{\partial u_i}{\partial \boldsymbol{n}_R}\right\|_{H^{k-\frac{3}{2}}(\partial K_R)}\right).\end{aligned}$$

Proof The proof is analogous to the one for Theorem 6.3, and we refer to [42, Sect. 6.1] for details. □

Considering Theorems 6.3 and 6.4 together, we get the following global result (where we consider ∂K_R to be a circle and thus C^∞):

Theorem 6.5 *Let Assumptions 2.3 and 2.4 hold and let the nominal radius r_0 belong to $C^k_{per}([0, 2\pi))$, with k as in Lemma 2.5. Let the map Φ be given by (3.2) with the mollifier fulfilling Assumption 3.3. Moreover, let the interface $\hat{\Gamma}$ be $C^{k-1,1}$. If k as in Lemma 2.5 is such that $k \geq 2$, then $\hat{u}$ belongs to $H^k(K_R \cap \hat{D}_1) \cup H^k(\hat{D}_2)$ and*

$$\|\hat{u}(\boldsymbol{y})\|_{H^k(K_R\cap\hat{D}_1)} + \|\hat{u}(\boldsymbol{y})\|_{H^k(\hat{D}_2)} \leq C\|\hat{u}(\boldsymbol{y})\|_{H^1(K_R)},$$

with $C = C(a_-, \mathcal{K}, k, |K_R|)$ independent of $J \in \mathbb{N}$ and of $\boldsymbol{y} \in \mathcal{P}_J$. In particular, if Assumption 4.4 holds, then we have the J- and $\boldsymbol{y}$-independent bound

$$\|\hat{u}(\boldsymbol{y})\|_{H^k(K_R\cap\hat{D}_1)} + \|\hat{u}(\boldsymbol{y})\|_{H^k(\hat{D}_2)} \leq \tilde{C}\left(\|u_i\|_{H^{k-\frac{1}{2}}(\partial K_R)} + \left\|\frac{\partial u_i}{\partial \boldsymbol{n}_R}\right\|_{H^{k-\frac{3}{2}}(\partial K_R)}\right), \tag{6.4}$$

with $\tilde{C} = \tilde{C}(R, a_-, \mathcal{K}, k, |K_R|)$*, and* a_-*,* $\mathcal{K}$ *defined as in Corollary 6.3.*

Remark 6.6 As it is evident from (2.3), we have that $k \to \infty$ as $p \to 0$.

Remark 6.7 Theorem 6.5 holds not only for the map (3.2), but for any map satisfying Assumption 3.1 with k as in Lemma 2.5.

Remark 6.8 In the case of the mapping (3.2) with the mollifier given by (3.3), we treat $\partial \hat{D}_2^{in}$ as an additional interface with homogeneous transmission conditions, across which the coefficients are discontinuous because of the jump of the Jacobian matrix of Φ. Proceeding as before, we obtain

$$\|\hat{u}(\boldsymbol{y})\|_{H^k(K_R \cap \hat{D}_1)} + \|\hat{u}(\boldsymbol{y})\|_{H^k(\hat{D}_2 \setminus \hat{D}_2^{in})} + \|\hat{u}(\boldsymbol{y})\|_{H^k(\hat{D}_2^{in})} \leq \tilde{C} \left(\|u_i\|_{H^{k-\frac{1}{2}}(\partial K_R)} + \left\| \frac{\partial u_i}{\partial \boldsymbol{n}_R} \right\|_{H^{k-\frac{3}{2}}(\partial K_R)} \right), \tag{6.5}$$

with constants defined as in (6.4).

6.2 Convergence of the fully discrete solution

The results stated in Theorems 5.3 and 5.4 assume that the solution $\hat{u} = \hat{u}(\boldsymbol{y})$ to (4.2) at the interpolation/quadrature points can be computed exactly, which is usually not the case in applications. Here we study instead the convergence of the sparse interpolation/quadrature operators coupled to a finite element discretization to compute the realizations. We consider a simplicial, quasi-uniform mesh on K_R, and assume that at ∂K_R the exact DtN map is available. Since we use a conforming discretization, for every realization existence, uniqueness and stability of the discrete solution are inherited from the continuous case.

Throughout this subsection, $k \in \mathbb{N}$ denotes the spatial regularity of the exact solution as from Theorem 6.5.

6.2.1 Convergence estimate for fixed finite element discretization

We first observe that:

Lemma 6.9 *Let Assumptions 4.4 and 5.11 hold, the former with* $\tau < T$ *and* T *as in Lemma 4.5. Then the discrete finite element solution* $\hat{u}_h(\boldsymbol{y})$ *to* (4.2) *admits an analytic extension* $\hat{u}_h(\boldsymbol{z})$ *to the complex domain, with the same domain of analyticity* $\mathcal{O}_{\boldsymbol{\rho}}$ *as the exact solution* $\hat{u}(\boldsymbol{y})$ *(*$\mathcal{O}_{\boldsymbol{\rho}}$ *as defined in* Eq. (5.10)*, with* $\boldsymbol{\rho}$ *a* $(\boldsymbol{b}, \varepsilon)^*$*-admissible sequence).*

Proof Since the Galerkin solution still satisfies the variational formulation (4.2) on the discrete, finite-dimensional space, $V_h \subset V$, the proof is the same as for Lemma 5.17. □

The convergence estimate for the fully discrete solution follows then simply applying the triangle inequality:

Theorem 6.10 *Let $I_\Lambda \hat{u}_h$ and $Q_\Lambda \hat{u}_h$ denote the solutions obtained respectively from sparse interpolation and quadrature of the discrete solution $\hat{u}_h$ to (4.2). Assume that the univariate interpolation and quadrature operators fulfill Assumption 5.1. Moreover, let Assumptions 4.4 and 5.11 be fulfilled. Assume that the same finite element discretization is used for all parameter realizations $\boldsymbol{y}_\nu$, $\nu \in \Lambda$, with polynomial order q and N_{dof} degrees of freedom, and that a q-th order boundary approximation is used for the interface $\hat{\Gamma}$ and ∂K_R.*

Then there exists a downward closed set Λ of cardinality at most N such that

$$\|\hat{u} - I_\Lambda \hat{u}_h\|_{L^\infty(\mathcal{P}_J, V)} \leq C N_{dof}^{-\frac{\min(k-1,q)}{2}} + C_1 N^{-s}, \quad s = \tfrac{1}{p} - 2, \tag{6.6}$$

$$\|\mathcal{I}(\hat{u}) - Q_\Lambda \hat{u}_h\|_V \leq C N_{dof}^{-\frac{\min(k-1,q)}{2}} + C_2 N^{-s}, \quad s = \tfrac{1}{p} - 2. \tag{6.7}$$

with $k \geq 1$ and $s, C, C_1, C_2 > 0$ independent of N, N_{dof}, of the truncation dimension $J \in \mathbb{N}$ and of $\boldsymbol{y} \in \mathcal{P}_J$.

Proof We apply the triangle inequality:

$$\|\hat{u}(\boldsymbol{y}) - I_\Lambda \hat{u}_h(\boldsymbol{y})\|_V \leq \|\hat{u}(\boldsymbol{y}) - \hat{u}_h(\boldsymbol{y})\|_V + \|\hat{u}_h(\boldsymbol{y}) - I_\Lambda \hat{u}_h(\boldsymbol{y})\|_V. \tag{6.8}$$

The first term is bounded using classical finite element results (see e.g. [34], where the interface problem is considered) together with (6.4) in Theorem 6.5, while the second term is bounded using Lemma 6.9 and Theorem 5.3. The result for the quadrature case is obtained in an analogous way using Theorem 5.4 to bound the second term. □

6.2.2 *Convergence estimate for parameter-adaptive discretization*

The idea is to distinguish the finite element error contribution for each difference operator Δ_ν^I as defined in (5.2) and (5.5) for the interpolation case, or Δ_ν^Q as defined in (5.2) and (5.6) for the quadrature case. The approach is the same as the one followed in [45] for the Legendre coefficients.

In the following theorem, we denote by $\boldsymbol{H}_l(\boldsymbol{y})$ the multivariate hierarchical polynomial associated with the node $\boldsymbol{y}_l$ in the case of nested sequences of interpolation points (see [9] for details). Also, $\left\{\boldsymbol{y}_l \in \Delta_\nu^I\right\}$ (resp. $\left\{\boldsymbol{y}_l \in \Delta_\nu^Q\right\}$) indicates the set of new interpolation (resp. quadrature) points introduced by the difference operator Δ_ν^I (resp. Δ_ν^Q), w_l denotes the quadrature weight associated with $\boldsymbol{y}_l$ and $\mathbb{L}_{\mathcal{R}_\nu}$ is the Lebesgue constant of the interpolation operator $I_{\mathcal{R}_\nu}$ on $\mathcal{R}_\nu := \{\mu \in \mathcal{F} : \mu < \nu\}$.

Theorem 6.11 *Let $I_\Lambda \hat{u}_{h,\Lambda}$ and $Q_\Lambda \hat{u}_{h,\Lambda}$ denote the solutions obtained respectively from sparse interpolation and quadrature of the discrete solution $\hat{u}_{h,\Lambda}$ to (4.2).*

Assume that the univariate interpolation and quadrature operators fulfill Assumption 5.1. Let Assumptions 4.4 and 5.11 be fulfilled. Let us denote by q_l and $N_{dof,l}$ the polynomial order and number of degrees of freedom used to compute the solution $\hat{u}_{h,\Lambda}(\boldsymbol{y}_l)$ at the interpolation/quadrature point $\boldsymbol{y}_l$. Furthermore, let us suppose that, for each realization $\boldsymbol{y}_l$, a q_l-th order boundary approximation is used for the interface $\hat{\Gamma}$ and ∂K_R.

Then there exists a downward closed set Λ of cardinality at most N such that

$$\|\hat{u} - I_\Lambda \hat{u}_{h,\Lambda}\|_{L^\infty(\mathcal{P}_J,V)} \leq \sum_{\nu\in\Lambda} \|\Delta_\nu^I(\hat{u} - \hat{u}_{h,\Lambda})\|_{L^\infty(\mathcal{P}_J,V)} + C_1 N^{-s}, \quad s = \tfrac{1}{p} - 2, \tag{6.9}$$

$$\|\mathcal{I}(\hat{u}) - Q_\Lambda \hat{u}_{h,\Lambda}\|_V \leq \sum_{\nu\in\Lambda} \|\Delta_\nu^Q(\hat{u} - \hat{u}_{h,\Lambda})\|_V + C_2 N^{-s}, \quad s = \tfrac{1}{p} - 2, \tag{6.10}$$

with $s, C_1, C_2 > 0$ independent of N, N_{dof}, of $J \in \mathbb{N}$ and of $\boldsymbol{y} \in \mathcal{P}_J$.

If the sequences $(\zeta_i)_{i\geq 0}$ of interpolation/quadrature points are nested, then the addends in the first sum satisfy, for the interpolation and quadrature case respectively:

$$\|\Delta_\nu^I(\hat{u} - \hat{u}_{h,\Lambda})\|_{L^\infty(\mathcal{P}_J,V)} \leq (1 + \mathbb{L}_{\mathcal{R}_\nu}) C(k) \cdot \sum_{\boldsymbol{y}_l \in \Delta_\nu^I} \|\boldsymbol{H}_l(\cdot)\|_{L^\infty(\mathcal{P}_J)} N_{dof,l}^{-\frac{\min(k-1,q_l)}{2}} \|\hat{u}(\boldsymbol{y}_l)\|_{H^k(K_R\cap\hat{D}_1)\cup H^k(\hat{D}_2)} \tag{6.11}$$

$$\|\Delta_\nu^Q(\hat{u} - \hat{u}_{h,\Lambda})\|_V \leq C(k) \sum_{\boldsymbol{y}_l \in \Delta_\nu^Q} |w_l| N_{dof,l}^{-\frac{\min(k-1,q_l)}{2}} \|\hat{u}(\boldsymbol{y}_l)\|_{H^k(K_R\cap\hat{D}_1)\cup H^k(\hat{D}_2)}, \tag{6.12}$$

with C independent of N, N_{dof}, of $J \in \mathbb{N}$ and of $\boldsymbol{y} \in \mathcal{P}_J$. The Lebesgue constant is bounded by $\mathbb{L}_{\mathcal{R}_\nu} \leq (\sharp\mathcal{R}_\nu)^{\theta+1}$.

We recall that $\|\boldsymbol{H}_l(\cdot)\|_{L^\infty(\mathcal{P}_J)} \geq 1$ for every sequence of interpolation points and $\|\boldsymbol{H}_l(\cdot)\|_{L^\infty(\mathcal{P}_J)} = 1$ for every l in the case of Leja points on the real interval $[-1, 1]$ (see e.g. [11] for their definition).

Proof We first consider the interpolation case. Simply applying the triangle inequality:

$$\begin{aligned}\|\hat{u} - I_\Lambda \hat{u}_{h,\Lambda}\|_{L^\infty(\mathcal{P}_J,V)} &\leq \|\hat{u} - I_\Lambda \hat{u}\|_{L^\infty(\mathcal{P}_J,V)} + \|I_\Lambda \hat{u} - I_\Lambda \hat{u}_{h,\Lambda}\|_{L^\infty(\mathcal{P}_J,V)} \\ &\leq \|\hat{u} - I_\Lambda \hat{u}\|_{L^\infty(\mathcal{P}_J,V)} + \sum_{\nu\in\Lambda} \|\Delta_\nu^I \hat{u} - \Delta_\nu^I \hat{u}_{h,\Lambda}\|_{L^\infty(\mathcal{P}_J,V)};\end{aligned}$$

thanks to Lemma 5.17, Theorem 5.3 holds and thus we get (6.9).

If the sequence of interpolation points is nested, then, according to [9, Formula (2.25)], one can write, for a generic element $g \in L^\infty(\mathcal{P}_J, V)$,

$$\Delta_\nu^I g(\boldsymbol{y}) = \sum_{\boldsymbol{y}_l \in \Delta_\nu^I} \left(g(\boldsymbol{y}_l) - I_{\mathcal{R}_\nu} g(\boldsymbol{y}_l)\right) \boldsymbol{H}_l(\boldsymbol{y})$$

(with $I_{\mathcal{R}_\nu}$ the interpolation operator on $\mathcal{R}_\nu$). Thus, for each $\nu \in \Lambda$:

$$\begin{aligned}
&\|\Delta_\nu^I \hat{u} - \Delta_\nu^I \hat{u}_{h,\Lambda}\|_{L^\infty(\mathcal{P}_J,V)} \\
&\leq \sum_{\boldsymbol{y}_l \in \Delta_\nu^I} \|\hat{u}(\boldsymbol{y}_l) - \hat{u}_{h,\Lambda}(\boldsymbol{y}_l) - I_{\mathcal{R}_\nu}(\hat{u}(\boldsymbol{y}_l) - \hat{u}_{h,\Lambda}(\boldsymbol{y}_l))\|_V \|\boldsymbol{H}_l(\cdot)\|_{L^\infty(\mathcal{P}_J)} \\
&\leq \sum_{\boldsymbol{y}_l \in \Delta_\nu^I} (1 + \mathbb{L}_{\mathcal{R}_\nu}) \|\hat{u}(\boldsymbol{y}_l) - \hat{u}_{h,\Lambda}(\boldsymbol{y}_l)\|_V \|\boldsymbol{H}_l(\cdot)\|_{L^\infty(\mathcal{P}_J)} \\
&\leq (1 + \mathbb{L}_{\mathcal{R}_\nu}) C(k) \sum_{\boldsymbol{y}_l \in \Delta_\nu^I} N_{dof,l}^{-\frac{\min(k-1,q_l)}{2}} \|\hat{u}(\boldsymbol{y}_l)\|_{H^k(K_R \cap \hat{D}_1) \cup H^k(\hat{D}_2)} \|\boldsymbol{H}_l(\cdot)\|_{L^\infty(\mathcal{P}_J)},
\end{aligned}$$

obtaining (6.11). Under the hypothesis on the Lebesgue constant for the univariate operator, we have that $\mathbb{L}_{\mathcal{R}_\nu} \leq (\sharp \mathcal{R}_\nu)^{\theta+1}$ and thus it grows with $\sharp \mathcal{R}_\nu$.

The result for the quadrature operator follows the same lines. The difference is, of course, in the definition of the difference operators for nested sequences: for a continuous $g \in L^1(\mathcal{P}_J, V)$, $\Delta_\nu^Q g = \sum_{\boldsymbol{y}_l \in \Delta_\nu^Q} w_l g(\boldsymbol{y}_l)$, and thus

$$\|\Delta_\nu^Q \hat{u} - \Delta_\nu^Q \hat{u}_{h,\Lambda}\|_V \leq C(k) \sum_{\boldsymbol{y}_l \in \Delta_\nu^Q} |w_l| N_{dof,l}^{-\frac{\min(k-1,q_l)}{2}} \|\hat{u}(\boldsymbol{y}_l)\|_{H^k(K_R \cap \hat{D}_1) \cup H^k(\hat{D}_2)}.$$

□

We remark that the smoothness $s = \frac{1}{p} - 2$ in the parameter space and the spatial smoothness k of the exact solution are not independent, owing to Theorem 6.5. This is formalized in the following important corollary, obtained by combining Theorem 6.5 with Theorem 6.10 or Theorem 6.11:

Corollary 6.12 *Let $\mathcal{I}_\Lambda \hat{u}_h$, $Q_\Lambda \hat{u}_h$ $\mathcal{I}_\Lambda \hat{u}_{h,\Lambda}$, $Q_\Lambda \hat{u}_{h,\Lambda}$ as in Theorem 6.10 and 6.11 respectively. Let Assumptions 2.3 and 4.4 be fulfilled, and Φ given by (3.2) with the mollifier fulfilling Assumption 3.3.*

Then if the coefficient sequences $\mathcal{C} = (c_j)_{j \geq 1}$, $\mathcal{S} = (s_j)_{j \geq 1}$ satisfy Assumption 2.4 and the nominal radius r_0 belongs to $C^k_{per}([0, 2\pi))$, with k as below, then the estimates (6.6)–(6.7) and (6.11)–(6.12) hold with

$$k = \begin{cases} \left\lfloor \frac{1}{p} - 1 \right\rfloor & \text{if } \frac{1}{p} - 1 \text{ is not an integer,} \\ \frac{1}{p} - 2 & \text{otherwise.} \end{cases} \tag{6.13}$$

Remark 6.13 When using the mapping (3.2) with mollifier (3.3), Corollary 6.12 holds if we use a high order boundary approximation also for $\partial \hat{D}_2^{in}$.

Remark 6.14 In this paper, we have considered a given truncated expansion of the radius as starting point, cf. (2.1), and focused on sparse quadrature and interpolation errors and their robustness with respect to the parameter J. If the expansion (2.1) results from the truncation of an infinite sum, then an additional source of error has to be considered in (6.6)–(6.7) and (6.9)–(6.10) (when measuring the convergence with respect to the solution to (4.2) where the radius expansion is not truncated).

More precisely, a truncation error of $CJ^{-\left(\frac{1}{p}-2\right)}$ has to be added to right-hand sides of (6.6)–(6.7) and (6.9)–(6.10), where $C = C(p, \mathcal{C}, \mathcal{S}, R, a_-, |K_R|)$ is independent of $J \in \mathbb{N}$, see [18, Thm. 4.1] and [21, Sect. 3.2].

6.3 Convergence of linear output functionals

We extend here the results of the previous subsection to the case that we want to interpolate or compute moments of a linear output functional $F = F(\boldsymbol{y}, u)$. Let $\hat{F} = \hat{F}(\boldsymbol{y}, \hat{u})$ denote the functional F after change of coordinates to the nominal space.

Throughout this subsection, $k \in \mathbb{N}$ denotes the spatial regularity of the exact solution as from Theorem 6.5.

If the functional depended only on the solution $\hat{u}$, then, thanks to linearity, the analyticity of $\hat{F}$ would follow immediately from the analyticity of the solution and of the map Φ, with the same polyradii for the polyellipses. However, in general this is not the case, and, to make sure that the $(\boldsymbol{b}, p, \epsilon)^*$-holomorphy assumption is satisfied, we require:

Assumption 6.15 *The linear output functional $\hat{F} = \hat{F}(\boldsymbol{y}, \hat{u})$ admits an analytic extension to the complex plane, with the same domain of analyticity as the solution $\hat{u}$.*

In particular, this assumption is satisfied when

$$\hat{F}(\boldsymbol{y}, \hat{u}) = \int_{\hat{A}} \mathcal{L}_1(\hat{u}(\boldsymbol{y}))\, d\hat{\boldsymbol{x}}, \tag{6.14}$$

where $\hat{A} \subseteq K_R$ is a nonzero measure set and $\mathcal{L}_1$ is a first order linear differential operator of the form $\mathcal{L}_1(v) = \hat{a}_1(\boldsymbol{y}, \hat{\boldsymbol{x}}) \cdot \hat{\nabla} \hat{v} + \hat{b}_1(\boldsymbol{y}, \hat{\boldsymbol{x}}) \hat{v}$, with coefficients which are measurable with respect to $\hat{\boldsymbol{x}}$ and admit a holomorphic extension, with respect to the high-dimensional parameter, to the same domain of analyticity as $\hat{u}$.

We also require that the linear output functional is stable in the following sense:

Assumption 6.16 *The linear output functional $\hat{F}$ belongs to $(H^m(K_R))^*$ for an integer $m \leq 1$, i.e. there exist $C > 0$ such that*

$$\left|\hat{F}(\boldsymbol{y}, \hat{v})\right| \leq C \|\hat{v}\|_{H^m(K_R)}, \quad \text{for all } \hat{v} \in H^m(K_R), \tag{6.15}$$

with C independent of the truncation dimension $J \in \mathbb{N}$ and of $\boldsymbol{y} \in \mathcal{P}_J$ (but possibly on the radius R of K_R).

This assumption is fulfilled, at least for $m = 1$, by functionals of the form (6.14).

We denote by $\hat{F}_h := \hat{F}(\boldsymbol{y}, \hat{u}_h)$ and $\hat{F}_{h,\Lambda} := \hat{F}(\boldsymbol{y}, \hat{u}_{h,\Lambda})$ the value of $\hat{F}$ when evaluated on the discrete solutions $\hat{u}_h$ and $\hat{u}_{h,\Lambda}$, respectively (nonadaptive and adaptive case).

For the case of uniform finite element order, if $\hat{F} = \hat{F}(\hat{u})$ satisfies Assumption 6.15, also its discrete version $\hat{F}_h$ does, thanks to Lemma 6.9, and we have:

Theorem 6.17 *Let $\hat{F}$ be a linear output functional defined on the nominal configuration and satisfying Assumption 6.15. We denote by $I_\Lambda \hat{F}_h$ and $Q_\Lambda \hat{F}_h$ the solutions obtained respectively from sparse interpolation and sparse quadrature of $\hat{F}_h = \hat{F}(\boldsymbol{y}, \hat{u}_h(\boldsymbol{y}))$. Let the assumptions of Theorem 6.10 be satisfied.*

Then there exists a downward closed set Λ of cardinality at most N such that the following estimates hold:

$$\|\hat{F} - I_\Lambda \hat{F}_h\|_{L^\infty(\mathcal{P}_J,V)} \leq C N_{dof}^{-t} + C_1 N^{-s}, \quad s = \frac{1}{p} - 2, \tag{6.16}$$

$$\|\mathcal{I}(\hat{F}) - Q_\Lambda \hat{F}_h\|_V \leq C N_{dof}^{-t} + C_2 N^{-s}, \quad s = \frac{1}{p} - 2, \tag{6.17}$$

with $s, C, C_1, C_2 > 0$ independent of N, N_{dof}, of $J \in \mathbb{N}$ and of $\boldsymbol{y} \in \mathcal{P}_J$.

If $\hat{F}$ fulfills Assumption 6.16, then $t = \frac{\min(k-1,q)+1}{2}$ for $m \leq 0$, $t = \frac{\min(k-1,q)}{2}$ for $m = 1$, $k \geq 1$.

For the parameter-adaptive case:

Theorem 6.18 *Let $\hat{F}$ be a linear output functional defined on the nominal configuration and satisfying Assumption 6.15. We denote by $I_\Lambda \hat{F}_{h,\Lambda}$ and $Q_\Lambda \hat{F}_{h,\Lambda}$ the solutions obtained respectively from sparse interpolation and sparse quadrature of $\hat{F}_{h,\Lambda} = \hat{F}(\boldsymbol{y}, \hat{u}_{h,\Lambda}(\boldsymbol{y}))$. Let the assumptions of Theorem 6.11 be satisfied.*

Then there exists a downward closed set Λ of cardinality at most N such that

$$\|\hat{F} - I_\Lambda \hat{F}_{h,\Lambda}\|_{L^\infty(\mathcal{P}_J,V)} \leq \sum_{\nu \in \Lambda} \|\Delta_\nu^I(\hat{F} - \hat{F}_{h,\Lambda})\|_{L^\infty(\mathcal{P}_J,V)} + C_1 N^{-s}, \quad s = \frac{1}{p} - 2, \tag{6.18}$$

$$\|\mathcal{I}(\hat{F}) - Q_\Lambda \hat{F}_{h,\Lambda}\|_V \leq \sum_{\nu \in \Lambda} \|\Delta_\nu^Q(\hat{F} - \hat{F}_{h,\Lambda})\|_V + C_2 N^{-s}, \quad s = \frac{1}{p} - 2, \tag{6.19}$$

with $s, C_1, C_2 > 0$ independent of N, N_{dof}, of $J \in \mathbb{N}$ and of $\boldsymbol{y} \in \mathcal{P}_J$.

If the sequences $(\zeta_i)_{i \geq 0}$ of interpolation/quadrature points are nested, then the addends in the first sum satisfy, for the interpolation and quadrature case respectively:

$$\|\Delta_\nu^I(F - \hat{F}_{h,\Lambda})\|_{L^\infty(\mathcal{P}_J,V)} \leq (1 + \mathbb{L}_{\mathcal{R}_\nu})\, C(k) \cdot \sum_{\boldsymbol{y}_l \in \Delta_\nu^I} \|\boldsymbol{H}_l(\cdot)\|_{L^\infty(\mathcal{P}_J)} N_{dof,l}^{-t} \|\hat{u}(\boldsymbol{y}_l)\|_{H^k(K_R \cap \hat{D}_1) \cup H^k(\hat{D}_2)}, \tag{6.20}$$

$$\|\Delta_\nu^Q(F - \hat{F}_{h,\Lambda})\|_V \leq C(k) \sum_{\boldsymbol{y}_l \in \Delta_\nu^Q} |w_l| N_{dof,l}^{-t} \|\hat{u}(\boldsymbol{y}_l)\|_{H^k(K_R \cap \hat{D}_1) \cup H^k(\hat{D}_2)}, \tag{6.21}$$

with $C > 0$ independent of N, N_{dof}, of $J \in \mathbb{N}$ and of $\boldsymbol{y} \in \mathcal{P}_J$, and the Lebesgue constant bounded as in Theorem 6.11.

If $\hat{F}$ fulfills Assumption 6.16, then $t = \frac{\min(k-1,q)+1}{2}$ for $m \leq 0$, $t = \frac{\min(k-1,q)}{2}$ for $m = 1$, $k \geq 1$.

The proofs for the two theorems are analogous to the proofs of Theorem 6.10 and 6.11, respectively. The gain of one order of convergence in (6.16) and (6.20) is a standard result of finite element analysis using a duality argument (see e.g. [5]).

Remark 6.19 As noted in Remark 6.14 for the solution $\hat{u}$, in the case that (2.1) is obtained by the truncation of an infinite sum, then, in order to take into account the truncation error, an additional term on the right-hand sides of (6.16)–(6.17) and (6.18)–(6.19) should be added. Namely, the linearity of the output functional ensures that the truncation error is bounded by $\tilde{C}\, J^{-\left(\frac{1}{p}-2\right)}$, where, denoting by C the constant in (6.15), $\tilde{C} = \tilde{C}(p, \mathcal{C}, \mathcal{S}, R, a_-, |K_R|, C)$ is independent of $J \in \mathbb{N}$ [18, Sect. 2.3].

7 Numerical experiments

The geometry is as shown in Fig. 1, with a nominal, angle-independent radius of size $r_0 = 10$nm. We consider the transverse electric mode (TE), i.e. the solution u represents the component of the electric field which is perpendicular to the plane in which the equations are solved (plane of incidence); in this case $\alpha_2 = 1$ in (1.2). The incident wave u_i is coming from the left with an incidence angle 0 with respect to the horizontal axis ($\boldsymbol{d} = (1, 0)$), and frequency $f = 10^4$THz. The wavenumber in free space is $\kappa_0 = \frac{2\pi f}{c_0}$, with $c_0 = 3 \cdot 10^8$m/s the light speed. The scatterer is a dielectric with relative permittivity $\varepsilon_2 = 2$ and the surrounding medium is air ($\varepsilon_1 = 1$), so that $\kappa_1 = \kappa_0$ and $\kappa_2 = \kappa_0\sqrt{\varepsilon_2}$.

To compute interpolants and means of the quantities of interest, we use the sparse grid algorithm described in Section 5.2 (Algorithm 1) with $\vartheta = 1$.

As domain mapping, we use (3.2) with the mollifier (3.3).

For each experiment, we compare two choices for the univariate sequence $\left(\zeta_j^k\right)_{j=0}^{n_k}$ of interpolation/quadrature points:

- Clenshaw-Curtis (CC):

$$\begin{aligned} \zeta_0^k &= 0 \ \text{ if } n_k = 1 \\ \zeta_j^k &= -\cos\left(\frac{\pi j}{n_k - 1}\right), \ j = 0, \ldots, n_k - 1, \ \text{ if } n_k > 1, \end{aligned}$$

  with $n_0 = 1$ and $n_k = 2^k + 1$, for $k \geq 1$;
- $\mathfrak{R}$-Leja sequence (RL): projection on $[-1, 1]$ of a Leja sequence for the complex unit disk initiated at 1:

$$\begin{aligned} &\zeta_0^k = 0, \zeta_1^k = 1, \zeta_2^k = -1, \ \text{ if } j = 0, 1, 2, \\ &\zeta_i^k = \mathfrak{R}(\hat{z}), \ \text{with } \hat{z} = \operatorname{argmax}_{|\zeta|=1} \prod_{l=1}^{j-1} |\zeta - \zeta_l^k|, \ j = 3, \ldots, n_k, \ \text{ if } j \text{ odd}, \\ &\zeta_i^k = -\zeta_{j-1}^k, \ j = 3, \ldots, n_k, \ \text{ if } j \text{ even}, \end{aligned}$$

  with $n_k = 2k + 1$, for $k \geq 0$, see [6].

The Clenshaw-Curtis and $\mathfrak{R}$-Leja points satisfy Assumption 5.1.

The finite element solutions are computed using the C++ NGSolve library,[2] providing high order elements for any shape; NGSolve has been linked to the MKL version of the PARDISO library to compute the solution of the resulting algebraic system.

To truncate the domain and approximate the DtN map, we consider a circular Perfectly Matched Layer (PML, see [3, 15]) around the boundary ∂K_R; for every $\boldsymbol{y} \in \mathcal{P}_J$, the mapping $\Phi(\boldsymbol{y})$ is prolongated as the identity in the PML. In [33] it is shown that, if the fictitious absorption coefficient in the PML is properly chosen, then the PML can be used in the finite element framework to truncate the domain for Helmholtz equation in an almost reflectionless manner for all frequencies. We use a PML that starts at radius $R = 80$nm and ends at radius $R' = 110$nm, with absorption coefficient (or damping parameter) $\alpha = 0.5$ [15].

As Q.o.I.s, we consider the interpolation and quadrature of the real part of the solution to (4.2) and of the modulus of the far field pattern (defined below). In each of these four cases, we consider the expansion of the stochastic radius (2.1) for three variations of the sparsity parameter: $s_j = c_j = \frac{0.1 r_0}{j^{\frac{1}{p}}}$, $j \geq 1$, for $\frac{1}{p} = 2, 3, 4$. Moreover, for the interpolation and quadrature of the real part of the solution, for each value of the summability exponent p, we compare the cases $2J = 16$, $2J = 32$ and $2J = 64$, with $2J = d$ the dimension of the parameter space. The maximal shape variations with respect to r_0 are of the order of 22% for $\frac{1}{p} = 2$, 17% for $\frac{1}{p} = 3$ and 15% for $\frac{1}{p} = 4$ (for all the three truncations of the radius expansion). For the interpolation and quadrature of the far field pattern, instead, we only consider the truncation $2J = 16$, because of the higher computational effort needed to compute realizations for this Q.o.I..

For quadrature, the error $\|\mathcal{I}(g) - Q_\Lambda(g)\|_V$, where g is the Q.o.I., is computed considering as $\mathcal{I}(g)$ the reference solution obtained with the high order quasi-Monte Carlo algorithm described in [20] and [22], using 2^{16} quadrature points and $C = 0.1$ as bound on the Walsh coefficient. For the interpolation error $\sup_{\boldsymbol{y}\in\mathcal{P}_J} \|g - I_\Lambda(g)(\boldsymbol{y})\|_V$, the supremum is approximated calculating, at each of the 2^{16} points used by the high order quasi-Monte Carlo algorithm in the quadrature case, the difference between the realization of the Q.o.I and the value of the interpolant, and then taking the maximum error among the 2^{16} realizations. We will provide the explicit expression of the error (in particular defining the space V) for each of the cases considered. The reference solutions are computed on the same finite element space used for the Smolyak algorithm. The quadrature error is calculated for every iteration of the algorithm, while the interpolation error is calculated every 10 iterations, starting from the last one and going backward until the last iteration with number bigger or equal to 10.

[2] https://sourceforge.net/projects/ngsolve/

7.1 Test cases

7.1.1 Interpolation of the real part of the solution on the nominal configuration

To compute the finite element solution given a parameter realization, we have used globally continuous, piecewise 2-nd order polynomial ansatz functions on an unstructured, quasi-uniform triangulation, leading to a total of 37309 degrees of freedom (including the PML), and using a 2-nd order polynomial boundary approximation. The Smolyak interpolation has been applied to the part of the solution that is not inside the PML, corresponding to an array carrying 28415 degrees of freedom.

The error considered is $\sup_{\boldsymbol{y}\in\mathcal{P}_J} \|\mathrm{Re}\,\hat{u}_h(\boldsymbol{y}) - I_\Lambda(\mathrm{Re}\,\hat{u}_h)(\boldsymbol{y})\|_{H^1(K_R)}$. Figure 4 shows the forementioned interpolation error versus the cardinality of the index set Λ and versus the number of PDE solves. In Figure 5, instead, we compare, for each variation of the sparsity parameter, the performance of the algorithm for the three different dimensions of the parameter space considered.

7.1.2 Interpolation of the modulus of the far field pattern

Given a radiating solution $u_s = u - u_i$ to the Helmholtz equation, the far field pattern is a function defined on the unit circle S^1 describing the asymptotic behavior of $u_s(\boldsymbol{x})$ for $|\boldsymbol{x}| \to \infty$.

The far field mapping $F : H^1_{\mathrm{loc}}(\mathbb{R}^2) \to C^\infty(S^1)$ associates to a scattered wave u_s its far field pattern. It is given by [37, Formulae (3) and (5)]

$$F(u_s)(\hat{\boldsymbol{\xi}}) = C_F \int_\Sigma \left\{ u_s(\boldsymbol{x}) \frac{\partial G(\hat{\boldsymbol{\xi}}, \boldsymbol{x})}{\partial \boldsymbol{n}(\boldsymbol{x})} - \frac{\partial u_s}{\partial \boldsymbol{n}}(\boldsymbol{x}) G(\hat{\boldsymbol{\xi}}, \boldsymbol{x}) \right\} \mathrm{d}S(\boldsymbol{x}), \quad \hat{\boldsymbol{\xi}} \in S^1, \quad (7.1)$$

where Σ is a simple closed path around the scatterer and $\boldsymbol{n}$ its outward unit normal vector field. The function $G = G(\hat{\boldsymbol{\xi}}, \boldsymbol{x})$ describes the behavior of the Green's function when the modulus of the second argument tends to infinity (we refer to [16, Sect. 2.2] for details); for a particle in free space, $G(\hat{\boldsymbol{\xi}}, \boldsymbol{x}) = \frac{1}{4\pi} e^{-i\kappa_1 \hat{\boldsymbol{\xi}}\cdot\boldsymbol{x}}$ (with κ_1 the wavenumber in free space). C_F is a normalizing constant, set to $C_F = \sqrt{\frac{2\pi}{\kappa_1}} e^{i\frac{\pi}{4}}$.

A simple application of Green's formula shows that the far field pattern is independent of the path Σ chosen to enclose the scatterer. Thus, we can consider two circles Σ_1 and Σ_2 around the particle, with Σ_1 contained in Σ_2, and the annulus A enclosed between them, and choose a cut-off function $\psi \in C^2(A)$ such that

$$\psi|_{\Sigma_2} = 1, \quad \psi|_{\Sigma_1} = 0, \quad \nabla\psi|_{\Sigma_1} = \nabla\psi|_{\Sigma_2} = \boldsymbol{0}. \quad (7.2)$$

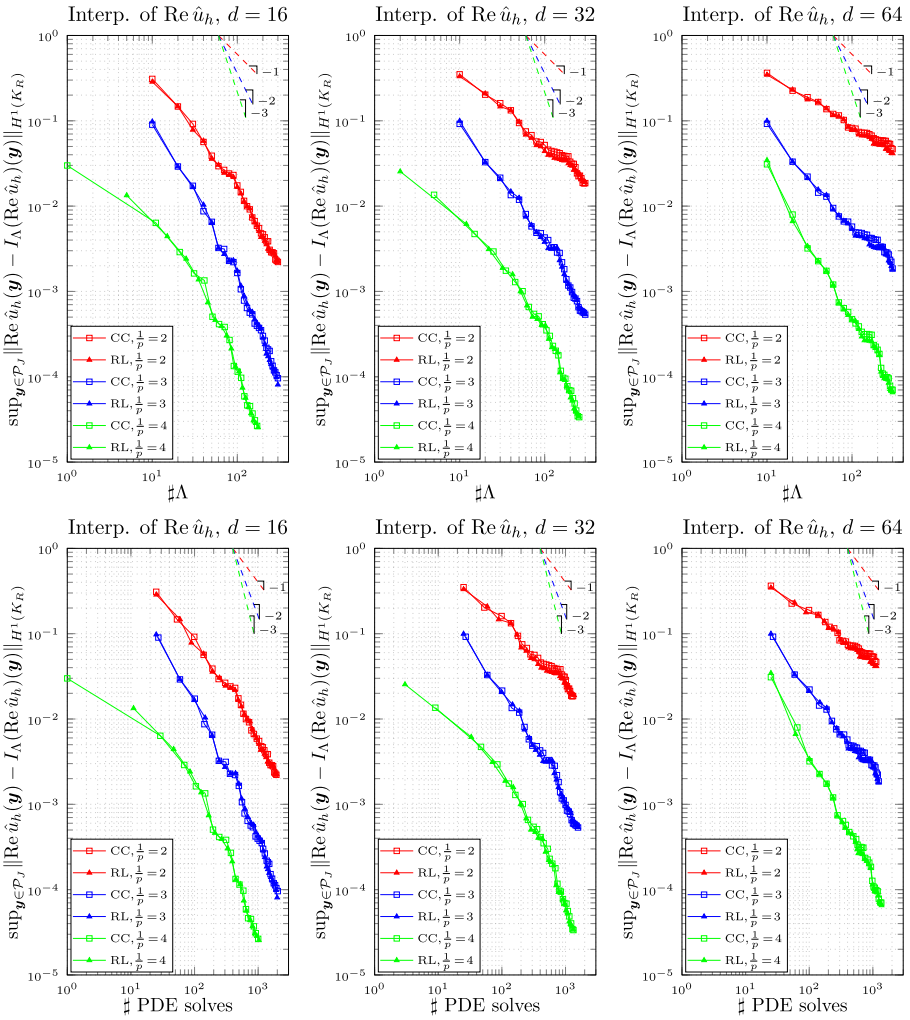

Fig. 4 Comparison of the errors for the interpolated solution with respect to the cardinality of the index set Λ (top) and to the number of PDE solves (bottom), using Clenshaw-Curtis and $\mathfrak{R}$-Leja points for 16 (left), 32 (middle) and 64 (right) dimensions. Maximal shape variations with respect to r_0 of about 22% for $\frac{1}{p} = 2$, 17% for $\frac{1}{p} = 3$ and 15% for $\frac{1}{p} = 4$

Applying Green's formula, it is easy to see [30] that (7.1) is equivalent to the modified far field mapping

$$F^*(u_s)(\hat{\boldsymbol{\xi}}) = C_F \int_A \nabla\psi(\boldsymbol{x}) \cdot \Big(u_s(\boldsymbol{x}) \nabla G(\hat{\boldsymbol{\xi}}, \boldsymbol{x}) - \nabla u_s(\boldsymbol{x}) G(\hat{\boldsymbol{\xi}}, \boldsymbol{x}) \Big)\, \mathrm{d}\boldsymbol{x}, \quad \hat{\boldsymbol{\xi}} \in S^1. \tag{7.3}$$

The advantage of formula (7.3) with respect to (7.1) is that, for fixed $\hat{\boldsymbol{\xi}} \in S^1$, $u_s \mapsto F^*(u_s)(\hat{\boldsymbol{\xi}})$ is a linear functional that is continuous on the energy space $H^1(A)$.

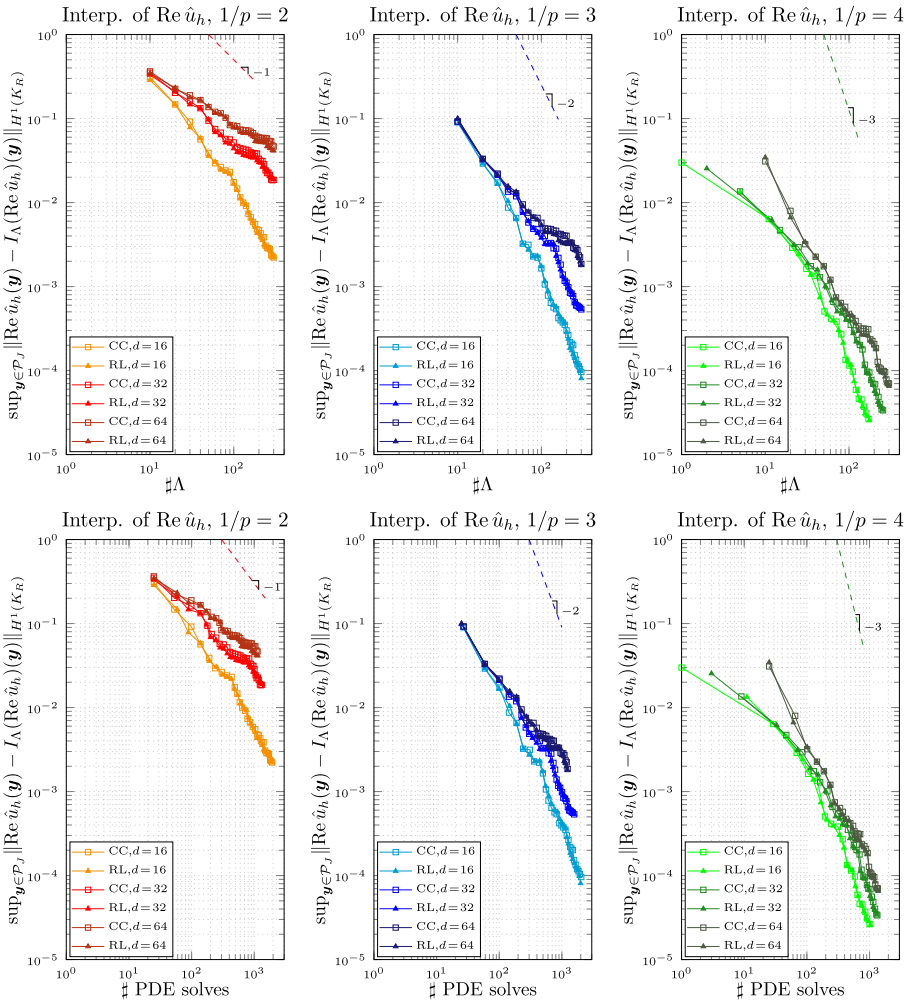

Fig. 5 Comparison of the errors for the interpolated solution with respect to the cardinality of the index set Λ (top) and to the number of PDE solves (bottom), using Clenshaw-Curtis and $\mathfrak{R}$-Leja points for variations of the sparsity parameter $\frac{1}{p} = 2$ (left), 3 (middle) and 4 (right). Maximal shape variations with respect to r_0 of about 22% for $\frac{1}{p} = 2$, 17% for $\frac{1}{p} = 3$ and 15% for $\frac{1}{p} = 4$

If we now apply the far field computation to the case when the scatterer has a stochastic boundary, we can fix an annular integration region $\hat{A}$ and a cut-off function $\hat{\psi}$ on the *nominal* domain $\hat{D}_1$, and (7.3) reads:

$$\begin{aligned}\hat{F}^*(\hat{u}_s(y))(\hat{\xi}) \;=\; & C_F \int_{\hat{A}} D\Phi(y)^{-\top}\hat{\nabla}\hat{\psi}(\hat{x}) \cdot \hat{u}_s(\hat{x}) D\Phi(y)^{-\top}\hat{\nabla}\hat{G}(\hat{\xi},\hat{x}) \mathrm{det} D\Phi(y)\,\mathrm{d}\hat{x} \\ & - \int_{\hat{A}} D\Phi^{-\top}(y)\hat{\nabla}\hat{\psi} \cdot D\Phi(y)^{-\top}\hat{\nabla}\hat{u}_s(\hat{x})\hat{G}(\hat{\xi},\hat{x})\mathrm{det} D\Phi(y)\,\mathrm{d}\hat{x}, \quad \hat{\xi} \in S^1,\end{aligned} \tag{7.4}$$

where $\Phi(\boldsymbol{y})$ is the mapping from the nominal configuration, as considered in the previous sections, $\hat{u}_s(\boldsymbol{y}, \hat{\boldsymbol{x}}) = \hat{u}(\boldsymbol{y}, \hat{\boldsymbol{x}}) - u_i(\Phi(\boldsymbol{y}, \hat{\boldsymbol{x}}))$ and $\hat{G}(\hat{\boldsymbol{\xi}}, \hat{\boldsymbol{x}}) = G(\hat{\boldsymbol{\xi}}, \Phi(\boldsymbol{y}, \hat{\boldsymbol{x}}))$. For each $\hat{\boldsymbol{\xi}} \in S^1$, the functional $\hat{F}^*(\hat{\boldsymbol{\xi}})$ satisfies Assumption 6.15 because Φ and $\hat{u}_s$ are analytic, and thus Theorems 6.17 and 6.18 hold. Moreover, if $\hat{\psi} \in C^2(\hat{A})$ and if Φ fulfills Assumption 3.1 with $k \geq 2$, integration by parts shows that, for fixed $\hat{\boldsymbol{\xi}} \in S^1$, the functional $\hat{F}^*(\hat{\boldsymbol{\xi}})$ fulfills Assumption 6.16 with $m = 0$; this means that, for each realization $\boldsymbol{y}$, we can expect the gain in one order for the finite element convergence as explained in the second part of Theorems 6.17 and 6.18.

When referring to the modulus of the farfield pattern, we mean its modulus as a complex-valued function for each $\hat{\boldsymbol{\xi}} \in S^1$. For the interpolation of $|\hat{F}^*(\hat{u}_s(\boldsymbol{y}))(\hat{\boldsymbol{\xi}})|$, $\hat{\boldsymbol{\xi}} \in S^1$, we consider the first 11 coefficients in its real Fourier expansion with respect to the angle $\varphi \in [0, 2\pi)$.

The annulus $\hat{A}$ has been chosen with inner radius 40nm and outer radius 70nm. For each realization, we have used a 2-nd order finite element space (with 2-nd order boundary approximation), carrying in total 33277 degrees of freedom, 13719 of which in the annulus region.

The results for the 16-dimensional case are shown in Fig. 6. Denoting by $\|\cdot\|_2$ the Euclidean norm, the error considered is $\sup_{\boldsymbol{y} \in \mathcal{P}_J} \|\hat{\mathbf{f}}_h(\hat{u}_h)(\boldsymbol{y}) - I_\Lambda(\hat{\mathbf{f}}_h(\hat{u}_h))(\boldsymbol{y})\|_2$, where $\hat{\mathbf{f}}_h$ denotes the vector of the approximated 11 Fourier coefficients.

7.1.3 Quadrature of the real part of the solution on the nominal configuration

For these experiments we have considered the quadrature on the nominal space. The finite element space is the same as in the interpolation case.

The error considered is $\|\mathcal{I}(\mathrm{Re}\,\hat{u}_h) - Q_\Lambda(\mathrm{Re}\,\hat{u}_h)\|_{H^1(K_R)}$. Figure 7 shows the quadrature error for different dimensions of the parameter space, versus the cardinality of the index set Λ and versus the number of PDE solves. Figure 8 shows instead, for each variation of the sparsity parameter, the comparison of the performance of the algorithm for dimension 16, 32 and 64 of the parameter space.

7.1.4 Quadrature of the modulus of the far field pattern

The finite element space is the same as in the interpolation case. The results are depicted in Fig. 9, where the error reported is $\|\mathcal{I}(\hat{\mathbf{f}}_h(\hat{u}_h)) - Q_\Lambda(\hat{\mathbf{f}}_h(\hat{u}_h))\|_2$ (with again $\mathbf{f}$ the vector of real Fourier coefficients).

7.2 Comments on the results of the numerical experiments

The results reported in the previous subsection show, in all the cases considered, that the empirical convergence rate is almost one order higher than the theoretical one, namely $s = \frac{1}{p} - 1$ in place of $s = \frac{1}{p} - 2$. This result is not new for anisotropic sparse interpolation and quadrature, as similar observations can be found in [43], which addresses Bayesian inversion for elliptic boundary value problems with unknown diffusion coefficient. Thus, it seems that the nonoptimality of the theory has not to

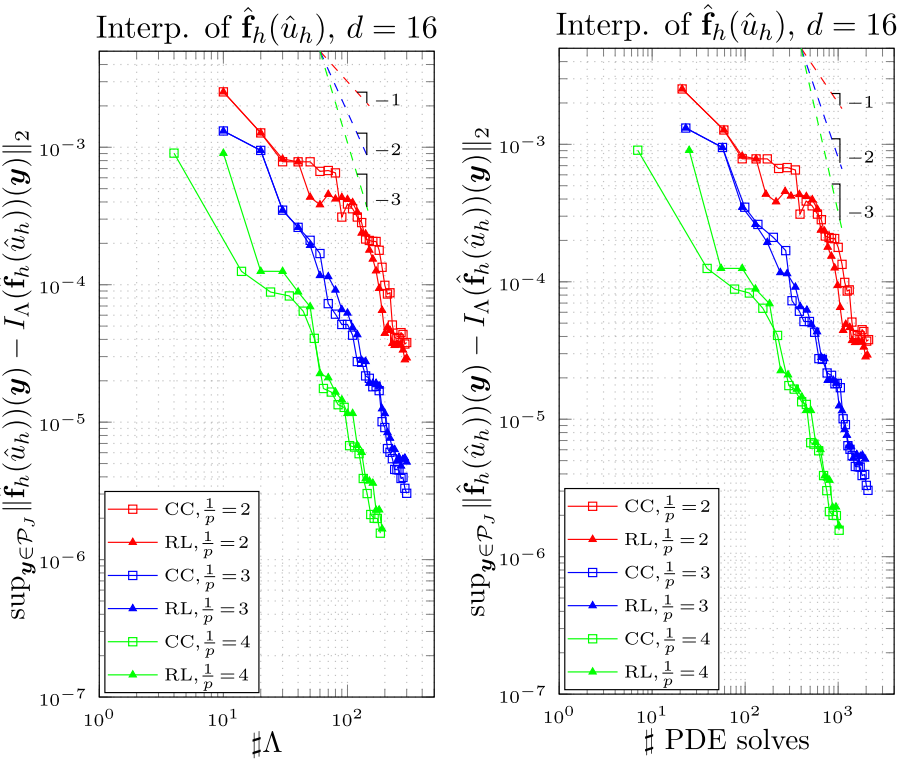

Fig. 6 Comparison of the errors for the interpolated far field Fourier coefficients with respect to the cardinality of the index set Λ (left) and the number of PDE solves (right), using Clenshaw-Curtis and $\mathfrak{R}$-Leja points for 16 dimensions. Maximal shape variations with respect to r_0 of 22% for $\frac{1}{p} = 2$, 17% for $\frac{1}{p} = 3$ and 15% for $\frac{1}{p} = 4$.

be found in our application to elliptic interface problems with random interface, but rather in the general theory for anisotropic sparse interpolation and quadrature. New results in this direction can be found in [50], see Remark 5.5.

Our numerical experiments confirm the dimension robustness of our algorithm, since, in each case, we observe the rate of at least $s = \frac{1}{p} - 1$ for all dimensions of the parameter space. Of course, the error is larger when more dimensions are activated, which is visible, in Figs. 5 and 8, in the right shift of the error plots when increasing the dimension of the parameter space. This is expected for two reasons. First, the rates stated in Section 5 are for a possibly infinite-dimensional parameter space. Yet, for a fixed, finite parametric dimension a dimension-dependent exponential convergence rate can be expected, which degenerates to the algebraic, dimension-independent rate of Theorem 5.20 as the number of dimensions increases; such behavior is particularly evident in the plot for $\frac{1}{p} = 2$ in Fig. 5. Second, the constants on the right-hand sides of (5.11) and (5.12) are dimension-independent upper bounds. When using a

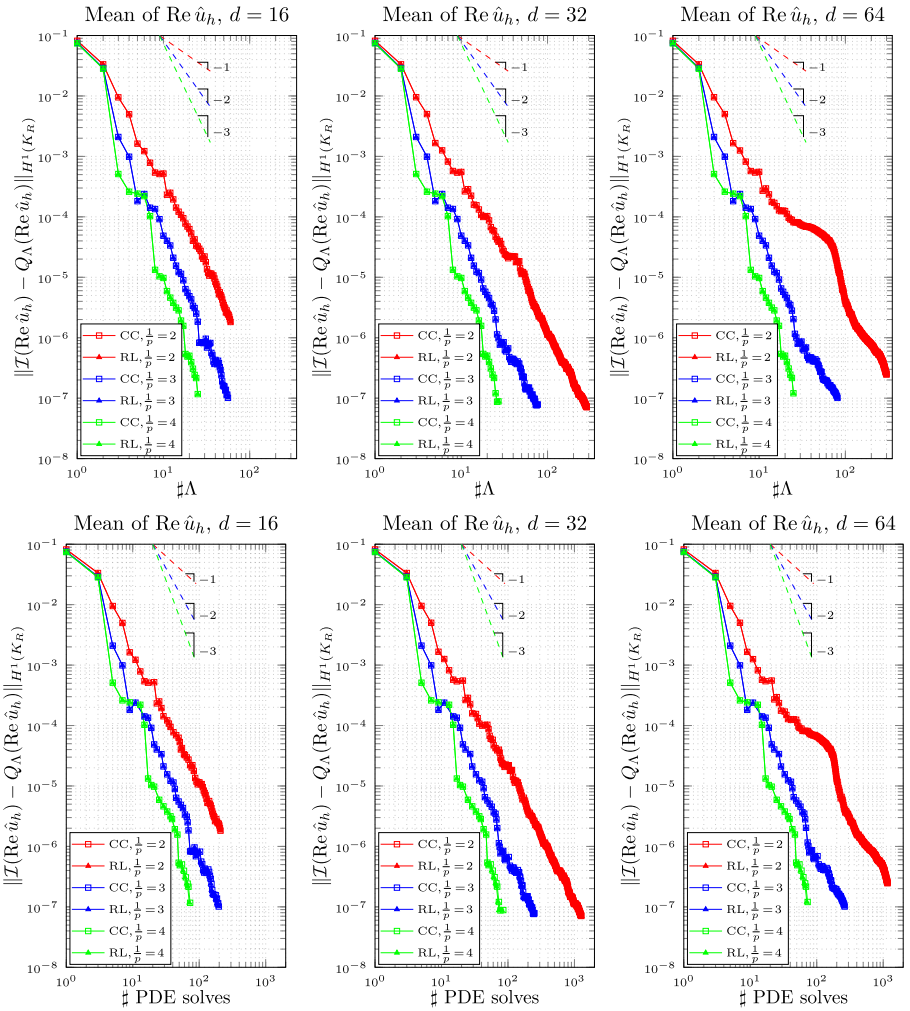

Fig. 7 Comparison of the errors for the quadrature of the real part of the solution with respect to the cardinality of the index set Λ (top) and to the number of PDE solves (bottom), using Clenshaw-Curtis and $\mathfrak{R}$-Leja points for 16 (left), 32 (middle) and 64 (right) dimensions. Maximal shape variations with respect to r_0 of about 22% for $\frac{1}{p} = 2$, 17% for $\frac{1}{p} = 3$ and 15% for $\frac{1}{p} = 4$

dimension truncation in the parameter space, then the actual constants may be significantly below their upper bounds and will increase parallel to the number of activated dimensions. The behavior of the exponential rate and of the multiplying constant with respect to the dimension of the parameter space is studied in detail in [26].

The plots also show that there is no significant difference in the performance of Clenshaw-Curtis and $\mathfrak{R}$-Leja points, also when considering the convergence with

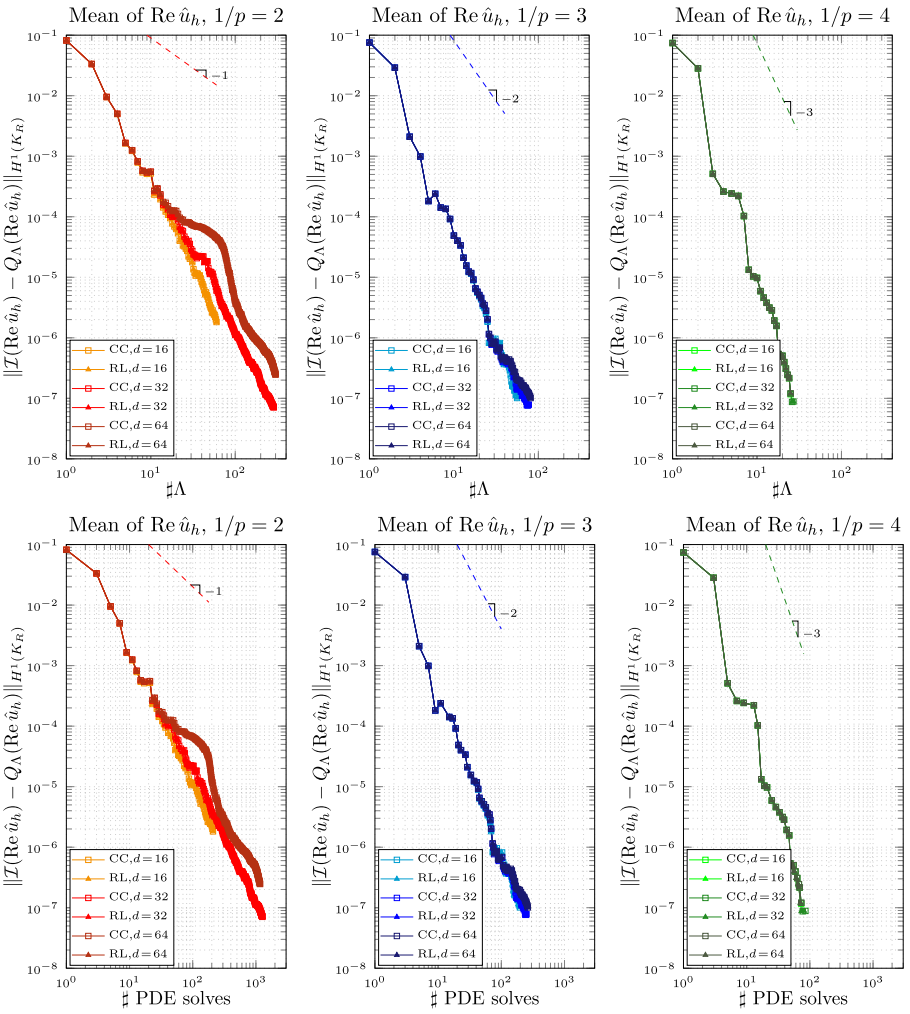

Fig. 8 Comparison of the errors for the quadrature of the real part of the solution with respect to the cardinality of the index set Λ (top) and to the number of PDE solves (bottom), using Clenshaw-Curtis and $\mathfrak{R}$-Leja points for variations of the sparsity parameter $\frac{1}{p} = 2$ (left), 3 (middle) and 4 (right). Maximal shape variations with respect to r_0 of about 22% for $\frac{1}{p} = 2$, 17% for $\frac{1}{p} = 3$ and 15% for $\frac{1}{p} = 4$

respect to the number of PDE solves. This is due to the fact that, although in the univariate case the number of Clenshaw-Curtis points increases exponentially with the order of the quadrature rule while the number of $\mathfrak{R}$-Leja points increases polynomially, when the index set contains indices associated with low order interpolation/quadrature operators, the number of PDE solves required by the two families of quadrature points do not differ significantly.

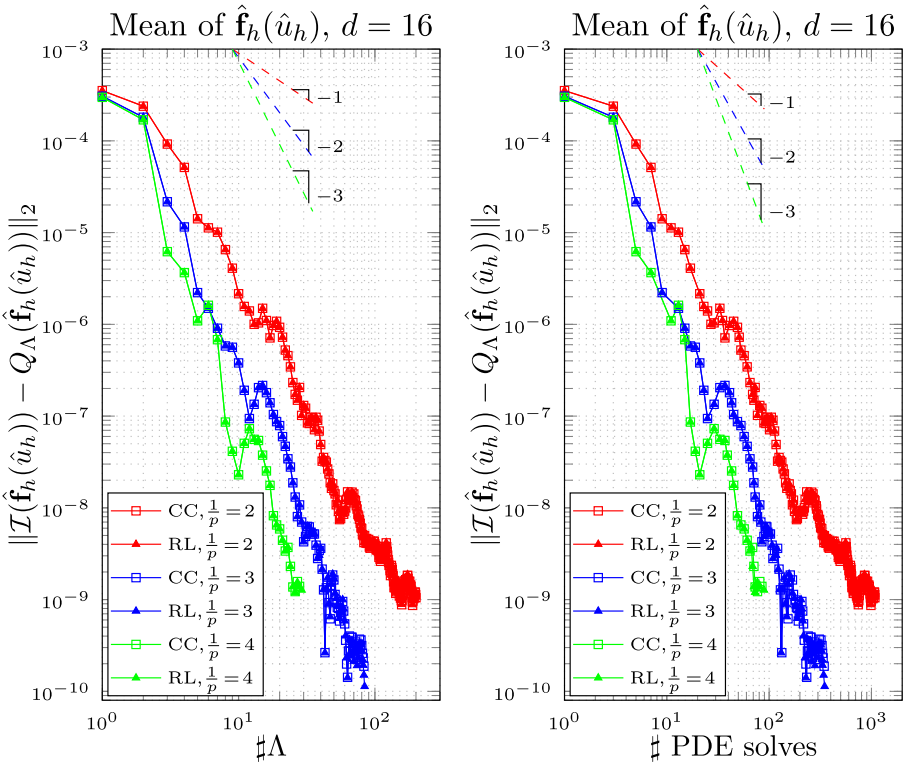

Fig. 9 Comparison of the errors for the quadrature of the far field Fourier coefficients with respect to the cardinality of the index set Λ (left) and the number of PDE solves (right), using Clenshaw-Curtis and $\mathfrak{R}$-Leja points for 16 dimensions. Maximal shape variations with respect to r_0 of 22% for $\frac{1}{p} = 2$, 17% for $\frac{1}{p} = 3$ and 15% for $\frac{1}{p} = 4$

8 Conclusions

We have presented a methodology for shape uncertainty quantification for the Helmholtz transmission problem, generalizable to any elliptic partial differential equation on a stochastic domain. The theory developed and the numerical experiments show that, under some regularity assumptions on the stochastic interface, it is possible to obtain high order, dimension independent convergence rates for the sparse interpolation and quadrature. We have also developed a regularity theory with respect to the spatial coordinates on the nominal domain, with norm bounds that are independent of the dimension truncation in the parameter space. The regularity results have been used to obtain convergence rates for the space discretization with finite elements, which, coupled to the results for sparse quadrature and interpolation, led to convergence estimates for the fully discretized solution.

Acknowledgments Research supported by ERC under Grant AdG247277 and by ETH under CHIRP Grant CH1-02 11-1.

References

1. Allaire, G., Jouve, F., Toader, A.-M.: A level-set method for shape optimization. C.R. Math. **334**, 1125–1130 (2002)
2. Babuška, I., Nobile, F., Tempone, R.: A stochastic collocation method for elliptic partial differential equations with random input data. SIAM Rev. **52**, 317–355 (2010)
3. Berenger, J.-P.: A perfectly matched layer for the absorption of electromagnetic waves. J. Comput. Phys. **114**, 185–200 (1994)
4. Bieri, M., Andreev, R., Schwab, C.: Sparse tensor discretization of elliptic SPDEs. SIAM J. Sci. Comput. **31**, 4281–4304 (2009)
5. Brenner, S.C., Scott, R.: The mathematical theory of finite element methods, vol. 15 Springer Science & Business Media (2008)
6. Calvi, J.-P., Manh, P.: Lagrange interpolation at real projections of Leja sequences for the unit disk. Proc. Am. Math. Soc. **140**, 4271–4284 (2012)
7. Canuto, C., Kozubek, T.: A fictitious domain approach to the numerical solution of PDEs in stochastic domains. Numerische mathematik **107**, 257–293 (2007)
8. Castrillon-Candas, J.E., Nobile, F., Tempone, R.F.: Analytic regularity and collocation approximation for PDEs with random domain deformations. Comput. Math. Appl. **71**, 1173–1197 (2016)
9. Chkifa, A., Cohen, A., Schwab, C.: High-dimensional adaptive sparse polynomial interpolation and applications to parametric PDEs. Found. Comput. Math. **14**, 601–633 (2014)
10. Chkifa, A.: Breaking the curse of dimensionality in sparse polynomial approximation of parametric PDEs. Journal de Mathé,matiques Pures et Appliquées **103**, 400–428 (2015)
11. Chkifa, M.A.: On the Lebesgue constant of Leja sequences for the complex unit disk and of their real projection. J. Approx. Theory **166**, 176–200 (2013)
12. Cohen, A., DeVore, R., Schwab, C.: Convergence rates of best N-term Galerkin approximations for a class of elliptic sPDEs. Found. Comput. Math. **10**, 615–646 (2010)
13. Cohen, A.: Analytic regularity and polynomial approximation of parametric and stochastic elliptic PDEs. Anal. Appl. **9**, 11–47 (2011)
14. Cohen, A., Schwab, C., Zech, J.: Shape Holomorphy of the stationary Navier-Stokes Equations, Report 2016-45, Seminar for Applied Mathematics, ETH Zürich, Switzerland. to appear in SIAM J. Math. Analysis (2016)
15. Collino, F., Monk, P.: The perfectly matched layer in curvilinear coordinates. SIAM J. Sci. Comput. **19**, 2061–2090 (1998)
16. Colton, D., Kress, R.: Inverse acoustic and electromagnetic scattering theory, vol. 93 Springer Science & Business Media (2012)
17. Dambrine, M., Harbrecht, H., Puig, B.: Computing quantities of interest for random domains with second order shape sensitivity analysis, ESAIM. Math. Model. Numer. Anal. **49**, 1285–1302 (2015)
18. Dick, J., Gantner, R.N., Le Gia, Q.T., Schwab, C.: Multilevel higher-order quasi-Monte Carlo Bayesian estimation. Math. Models Methods Appl. Sci. **27**, 953–995 (2017)
19. Eigel, M., Gittelson, C.J., Schwab, C., Zander, E.: Adaptive stochastic Galerkin FEM. Comput. Methods Appl. Mech. Eng. **270**, 247–269 (2014)
20. Gantner, R.N.: A generic C++ library for multilevel Quasi-Monte Carlo. In: Proceedings of the Platform for Advanced Scientific Computing Conference, PASC '16, pp. 11:1–11:12. ACM, New York (2016)
21. Gantner, R.N., Peters, M.D.: Higher order Quasi-Monte Carlo for Bayesian shape inversion, Report 2016-45, Seminar for Applied Mathematics, ETH Zürich, Switzerland (2016)
22. Gantner R.N., Schwab, C.: Computational higher order Quasi-Monte Carlo integration. In: Cools R., Nuyens, D. (eds.) Monte Carlo and Quasi-Monte Carlo Methods: MCQMC, Leuven, Belgium, April 2014, pp. 271–288. Springer International Publishing, Cham (2016)
23. Gerstner, T., Griebel, M.: Dimension–adaptive tensor–product quadrature. Computing **71**, 65–87 (2003)
24. Ghanem, R.G., Spanos, P.D.: Stochastic finite elements: a spectral approach Courier Corporation (2003)
25. Gilbarg, D., Trudinger, N.S.: Elliptic partial differential equations of second order, vol. 224 Springer Science & Business Media (2001)
26. Griebel, M., Oettershagen, J.: On tensor product approximation of analytic functions. J. Appr. Theory **207**, 348–379 (2016)

27. Harbrecht, H., Li, J.: First order second moment analysis for stochastic interface problems based on low-rank approximation. ESAIM: Math. Model. Numer. Anal. **47**, 1533–1552 (2013)
28. Harbrecht, H., Peters, M., Siebenmorgen, M.: Analysis of the domain mapping method for elliptic diffusion problems on random domains. Numer. Math. **134**, 823–856 (2016)
29. Harbrecht, H., Schneider, R., Schwab, C.: Sparse second moment analysis for elliptic problems in stochastic domains. Numer. Math. **109**, 385–414 (2008)
30. Hiptmair, R., Sargheini, S.: Scatterers on the Substrate: Far field formulas, Report 2015-02, Seminar for Applied Mathematics, ETH Zürich, Switzerland (2015)
31. Horn, R.A., Johnson, C.R.: Topics in matrix analysis. Cambridge University Press, Cambridge (1991)
32. Jerez-Hanckes, C., Schwab, C., Zech, J.: Electromagnetic wave scattering by random surfaces: Shape holomorphy. Math. Mod. Meth. Appl. Sci. **27**, 2229–2259 (2017)
33. Lassas, M., Somersalo, E.: On the existence and convergence of the solution of PML equations. Computing **60**, 229–241 (1998)
34. Li, J., Melenk, J.M., Wohlmuth, B., Zou, J.: Optimal a priori estimates for higher order finite elements for elliptic interface problems. Appl. Numer. Math. **60**, 19–37 (2010)
35. Li, R., Tang, T., Zhang, P.: Moving Mesh Methods in Multiple Dimensions Based on Harmonic Maps. J. Comput. Phys. **170**, 562–588 (2001)
36. McLean, W.C.H.: Strongly elliptic systems and boundary integral equations. Cambridge University Press, Cambridge (2000)
37. Monk, P., Süli, E.: The adaptive computation of far-field patterns by a posteriori error estimation of linear functionals. SIAM J. Numer. Anal. **36**, 251–274 (1998)
38. Nédélec, J.-C.: Acoustic and electromagnetic equations: integral representations for harmonic problems, vol. 144 Springer Science & Business Media (2001)
39. Nouy, A., Clement, A., Schoefs, F., Moës, N.: An extended stochastic finite element method for solving stochastic partial differential equations on random domains. Comput. Methods Appl. Mech. Eng. **197**, 4663–4682 (2008)
40. Osher S., Fedkiw, R.P.: Level set methods: An overview and some recent results. J. Comput. Phys. **169**, 463–502 (2001)
41. Paganini, A., Scarabosio, L., Hiptmair, R., Tsukerman, I.: Trefftz approximations: a new framework for nonreflecting boundary conditions. IEEE Trans. Magn. **PP**, 1–1 (2015)
42. Scarabosio, L.: Shape uncertainty quantification for scattering transmission problems, PhD thesis, ETH Zürich, 2016. Diss. No. 23574. http://e-collection.library.ethz.ch/eserv/eth:49652/eth-49652-02.pdf
43. Schillings, C., Schwab, C.: Sparse, adaptive Smolyak quadratures for Bayesian inverse problems. Inverse Prob. **29**, 065011 (2013)
44. Schillings, C., Schwab, C.: Sparsity in Bayesian inversion of parametric operator equations. Inverse Prob. **30**, 065007 (2014)
45. Schwab, C., Gittelson, C.J.: Sparse tensor discretizations of high-dimensional parametric and stochastic PDEs. Acta Numer. **20**, 291–467 (2011)
46. Tartakovsky, D.M., Xiu, D.: Stochastic analysis of transport in tubes with rough walls. J. Comput. Phys. **217**, 248–259 (2006)
47. Wiener, N.: The homogeneous chaos. Amer. J. Math. **60**(4), 897–936 (1938)
48. Xiu, D., Hesthaven, J.S.: High-order collocation methods for differential equations with random inputs. SIAM J. Sci. Comput. **27**, 1118–1139 (2005)
49. Xiu, D., Tartakovsky, D.M.: Numerical methods for differential equations in random domains. SIAM J. Sci. Comput. **28**, 1167–1185 (2006)
50. Zech, J., Schwab, C.: Convergence rates of high dimensional Smolyak quadrature, Report 2017-27, Seminar for Applied Mathematics, ETH Zürich, Switzerland (2017)